Universidad Autónoma de Sinaloa

Facultad de Ciencias Físico-Matemáticas

Lepton number violation in $\tau^- \to \pi^+\mu^-\mu^-\nu_\tau$ at Belle II experiment

Master Thesis

Lic. David Rodríguez Pérez

Supervisors

Dr. Pedro Luis Manuel Podesta Lerma

Dra. Isabel Domínguez Jiménez

2016

A mis padres,
Arturo y Felicitas,
gracias por todo.

Agradecimientos

Un logro más en mi vida y un buen día, pero no de los mejores. Los mejores días son cuando estoy con mi familia, con mis padres Arturo y Felicitas, mis hermanos Arturo y Miguel. En una reunión familiar los sabados por la tarde en casa de la abuela. Cuando sin esperar veo a un buen amigo. Como alvidar las platicas con mis maestros, Pedro Podesta e Isabel Domínguez, en las cuales además de lo académico también recibí buenos consejos y apoyo moral.

Este logro que fue posible a dos grandes instituciones. La Universidad Autónoma de Sinaloa, por el programa de maestría en Física así como a la planta docente capaz de impartirlo. Conacyt, por el apoyo económico brindado durante todo el tiempo de maestría. Gracias.

Abstract

In this work we study the possibility to find the $\tau^- \to \pi^+\mu^-\mu^-\nu_\tau$ channel in the Belle II detector, located in KEKB laboratory. This channel violate the leptonic number by two units and if found, it would be a proof of the Majorana nature of the neutrinos. However, up to this day the experiment have not started and all data used in this work have been simulated. In order to have an approximation to real experiment or real data we used two set of variables: *Reconstruction data* and *Simulation data*. We considered the transverse momentum, pseudorapidity, and polar angle distributions to reconstruct as well as possible the generated events. Furthermore, we considered $\tau^- \to \pi^+\mu^-\mu^+\nu_\tau$ and $\tau^- \to \pi^+\pi^-\pi^-\nu_\tau$ channels as background. We generated 50000 events for each channel using the KKMC generator.

Resumen

En este trabajo estudiamos la posibilidad de encontrar el decaimiento $\tau^- \to \pi^+\mu^-\mu^-\nu_\tau$ en el detector Belle II, localizado en el laboratorio KEKB. Este canal viola el número leptónico por dos unidades y de ser encontrado, sería una prueba de la naturaleza Majorana de los neutrinos. Sin embargo, hasta el día de hoy el experimento no ha iniciado y todos los datos usados en este trabajo han sido simulados. Con el fin de tener una aproximación a los datos reales dos conjuntos de variables son usados: *Reconstruction data* y *Simulation data*. Consideramos las distribuciones de momento transverso, pseudorapidez y ángulo polar para reconstruir los eventos lo mejor posible. Además, consideramos como ruido los siguientes decaimientos $\tau^- \to \pi^+\mu^-\mu^+\nu_\tau$ y $\tau^- \to \pi^+\pi^-\pi^-\nu_\tau$. Generamos 50000 eventos para cada canal usando el generador Monte Carlo KKMC.

Contents

List of Figures

List of Tables

Chapter 1

Introduction

In physics, detailed observation of the nature's behavior allows us to create mathematical models. Experiments based on this knowledge are the proof of the models and sometimes some of these last cannot survive due to discrepancies with reality. However, others can be improved in order to explain more physical phenomena; an example of this is the Standard Model (SM), theory about the fundamental structure of matter that was constructed through the years, our best understanding of three fundamental forces and fundamental particles, but not all. Some questions remain open about: gravity force, dark energy, dark matter, and more.

The SM is the current theory of fundamental particles and their interactions, which was created based on observations and theoretical predictions through several years. The questions about the origins of the universe and the formulation of matter allowed to develop the SM, using relativistic quantum field theory. In this theory all the elementary matter particles are fermions, interacting among themselves by the exchange of gauge bosons and the mass is generated by the Higgs mechanism.

There are four fundamental forces. However, the SM only describes three of them, the strong, weak and electromagnetic interactions but not gravitational interaction, yet. This, due to the fact that gravitation comes from a non perturbative theory.

There are two types of elementary matter particles, leptons and quarks. Whereas the quarks are confined due to the strong force, the leptons are unable to feel this force and thus they are not confined. However, both, charged leptons and quarks have gravitational, weak and electromagnetic interactions.

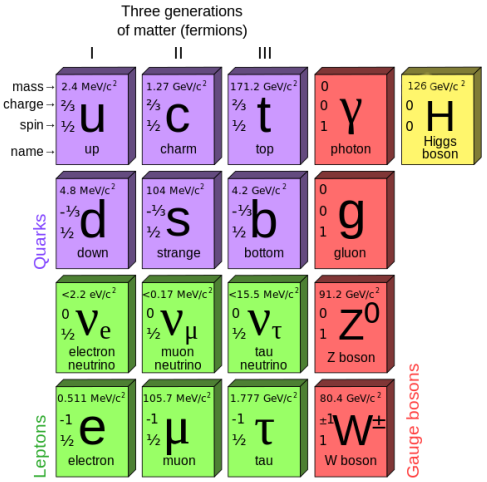

Figure 1.1: Standard Model.

The quarks are divided in 3 generations, as well as the leptons (Figure 1.1). Each generation contains a charge lepton e^-, μ^- or τ^-, with electric charge $-e_0 = -1.6 \times 10^{-19}$ C, and a corresponding neutral neutrino ν_e, ν_μ, or ν_τ. Quarks come in six flavors; the up-type quarks, u, c and t, have electric charge $+2e_0/3$, whereas the charge of the down-type quarks, d, s, and b, is $-e_0/3$.

In addition to the electric charge, quarks also have color charge. In the SM, the interaction between matter particles operates by exchanging force mediating particles.

In total, there are 12 mediator particles: eight gluons (g) for the strong force, three boson ($W^\pm$ and Z^0) for the weak force, and the photon (γ) for the electromagnetic force. Furthermore, the Higgs field generates the masses of the massive leptons and quarks (Figure 1.2).

1.1 Neutrinos

In recent years experiments with neutrinos [1][2] have questioned the SM since the SM considers that neutrinos are massless. Experiments with solar neutrinos [3] show that they oscillate from a definite color to another through long distances, and thus neutrinos should have mass [4]. However, in nature only left handed neutrinos have

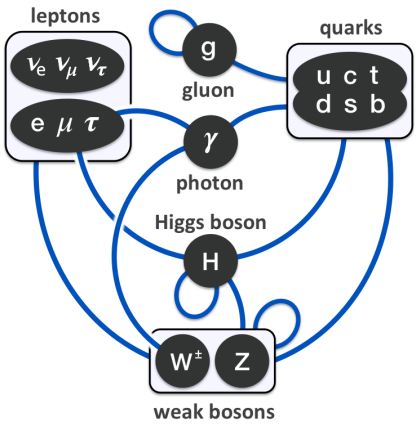

Figure 1.2: Interactions in the SM.

been observed [5] (right-handed anti-neutrinos) and then the mass term cannot be constructed. With this observation and considering the small neutrino masses, to consider the neutrino as massless particle seemed not to be a bad idea. But now it is necessary to modify the SM.

To consider the existence of right-handed neutrinos is one option, although they have not been observed. On the other hand, if neutrinos are Majorana particles we can write a mass term without right-handed neutrinos [6]. In the first option, the presence of right-handed neutrinos allows us to write one mass term in the weak Lagrangian, but we need to consider that the right-handed neutrino is very suppressed. The second option allows us to maintain only left-handed neutrinos, because neutrino and anti-neutrino are the same particle so we can write a mass term in the Lagrangian.

We focus our attention on the second option, looking for evidences that neutrino is indeed a Majorana particle. The non-conservation of lepton number will be the cornerstone in this study, decays in which the lepton number is not conserved in two units. The violation of lepton number will be the proof of the Majorana nature of the neutrinos [7].

This thesis is organized as follows. In Chapter II, we explain shortly Majorana neutrinos and their implication in the weak SM. In Chapter III, Belle II detector and its software description is given, in which we will find for signals of Majorana

neutrinos. In Chapter IV, we present the analysis and results of channels used in this work. Finally in Chapter V, Conclusions and future plans are discussed .

Chapter 2

Majorana neutrinos

Neutrinos are neutral particles of Standard Model that have half-integer spin, experiments suggest that neutrinos have mass but it is tiny compared to other subatomic particles. Furthermore, in the SM some conservation laws have emerged experimentally and not from theoretical restrictions, one of these laws is the *Lepton Number Conservation*. All leptons have assigned a value of +1, antileptons -1 and non-leptonic particles 0. Below, there is a brief overview of the β-decay and *Lepton Number Conservation* [4].

2.1 β-decay

In 1914 the continuous energy spectrum of electron from β decay was discovered. However, the β-decay was considered as a process of the transition of a nucleus with Z atomic number into a nucleus with $Z+1$ atomic number and the electron, and thus from the conservation of energy and momentum follows that the electron must have a fixed kinetic energy. In 1930 W. Pauli proposed the existence of a neutral particle with large penetration length, which he called initially "neutron". Later E. Fermi and E. Amaldi proposed to called Pauli's particle *neutrino*. After the discovery of neutron, in 1932 by Chadwick, E. Fermi solved quantitatively the problem of the continuous β-spectrum. He proposed a Hamiltonian similar to the electromagnetic interaction. For instance, the Hamiltonian of the electromagnetic interaction of protons is

$$\mathcal{H}_I^{EM}(x) = e\bar{p}(x)\gamma_\alpha p(x)A^\alpha(x) \tag{2.1}$$

where e is the electric charge of the proton, $p(x)$ is the proton field, $\bar{p}(x) = p^\dagger(x)\gamma^0$, $A^\alpha(x)$ is the electromagnetic field and γ_α are the Dirac matrices. In the β-decay

$$p \to n + e^+ + \nu \tag{2.2}$$

Fermi replaced the electromagnetic field by the positron-neutrino emission and the electric charge by an interaction constant, thus the β-decay Hamiltonian was

$$\mathcal{H}_I^\beta(x) = G_F\bar{p}(x)\gamma_\alpha n(x)\bar{e}(x)\gamma^\alpha\nu(x) + h.c. \tag{2.3}$$

in which $\bar{p}(x)\gamma_\alpha n(x)$ factor is the proton-neutron transition and $\bar{e}(x)\gamma^\alpha\nu(x)$ factor is the positron-neutrino emission, whereas G_F is the interaction constant. The Fermi Hamiltonian obey the Fermi rules [4]

$$\Delta I = 0;\ \Delta\pi = 0 \tag{2.4}$$

where I is spin and π is parity. However, β-decays which obey the Gamow-Teller rules were also observed

$$\Delta I = \pm 1,\ 0;\ \Delta\pi = 0. \tag{2.5}$$

This means that the Fermi Hamiltonian needs to be modified, thus the Hamiltonian will have the form

$$\mathcal{H}_I^\beta(x) = \sum_{i=S,V,T,A,P} G_i\bar{p}(x)O_i n(x)\bar{e}(x)O^i\nu(x) + h.c. \tag{2.6}$$

where $O \to 1,\ \gamma_\alpha,\ \sigma_{\alpha\beta},\ \gamma_\alpha\gamma_5,\ \gamma_5$ and G_i are coupling constants. The violation of parity in β-decay observed in experiments by Wu *et al.* in 1957 [8] limited the Hamiltonian as

$$\mathcal{H}_I^\beta(x) = \sum_{i=S,V,T,A,P} \bar{p}(x)O_i n(x)\bar{e}(x)O^i(G_i - G_i'\gamma_5)\nu(x) + h.c. \tag{2.7}$$

adding more coupling constants. In 1934 the neutrino mass was $m \leq 200$ eV but Landau, Lee and Yang and Salam proposed the two-component neutrino theory in which the neutrino mass is equal to zero. All fermion field can be written as

$$\Psi(x) = \Psi_L(x) + \Psi_R(x) \tag{2.8}$$

where

$$\Psi_{L,R}(x) = \frac{1 \mp \gamma_5}{2}\Psi(x) \tag{2.9}$$

and the main consequence, if neutrino mass is equal to zero, is

$$\Psi(x) = \Psi_R(x) \text{ or } \Psi_L(x). \tag{2.10}$$

In 1958 Goldhaber *et al.* [5] found that the helicity of neutrino is negative, and

$$\nu(x) = \nu_L(x). \tag{2.11}$$

And the equation 2.7 can be written as

$$\mathcal{H}_I^{\beta}(x) = \sum_{i=S,V,T,A,P} G_i \bar{p}_L O_i n_L \; \bar{e}_L O^i \nu_L + h.c. \tag{2.12}$$

or

$$\mathcal{H}_I^{\beta}(x) = G_F \bar{p}\gamma_\alpha(1-\gamma_5)n \; \bar{e}\gamma^\alpha(1-\gamma_5)\nu_L + h.c. \tag{2.13}$$

The Hamiltonian (2.13) is the simplest possible four-fermion Hamiltonian of the β-decay.

2.2 Lepton Number Conservation

The β-decay process was the cornerstone to know the weak interaction. The negative helicity of neutrino was very important to construct the Hamiltonian of the β-decay. But at the time when parity violation was discovered other weak processes involving a muon-neutrino pair were know

$$\mu^- + (A, Z) \rightarrow \nu + (A, Z-1) \tag{2.14}$$

$$\mu^+ \rightarrow e^+ + \nu + \bar{\nu} \tag{2.15}$$

where Z is the atomic number and A is the atomic mass. Then the question was, *Are these the same neutrinos that in β-decay?*

The non observation of the process

$$\mu \rightarrow e + \gamma \tag{2.16}$$

was the first indication that ν_e ($p \rightarrow n + e^+ + \nu$) and ν_μ ($\mu^- + (A, Z) \rightarrow \nu + (A, Z-1)$) were different. Then L. M. Lederman, M. Schwartz, J. Steinberger *et al.* [9] demonstrated that ν_e is different to ν_μ. Such experiment was realized in Brookhaven. The used neutrinos were generated by the $\pi \rightarrow \mu + \nu$ process. Then, these neutrinos were used to produce the process

$$\nu + N \rightarrow l + X \tag{2.17}$$

where N is an initial nucleus, X is a final nucleus and l is a resulting lepton. The result was always the same

$$\nu_\mu + N \rightarrow \mu + X \tag{2.18}$$

as result $\nu_e \neq \nu_\mu$.

These results and other experiments suggested the existence of a new quantum number, the *Lepton number (L)*, and its conservation

$$\sum_i L^{(i)} = conts. \tag{2.19}$$

2.3 Neutrino oscillations

In 1970 David *et al.* [10] with the Homestake experiment detected solar neutrinos. These neutrinos were ν_e's a product of nuclear fusion where the main contribution comes from the proton-proton reaction

$$p + p \rightarrow d + e^+ + \nu_e \tag{2.20}$$

predicted by the *Standard Solar Model*. However, the observed rate was 2-3 times smaller that the rate predicted. This discrepancy was called *the solar neutrino problem*. In 1988 the Kamiokande experiment [11], the first experiment in which the neutrino direction was measured, confirming the solar neutrino problem.

However, no indications in favor of neutrino oscillations were found in the eighties and nineties in numerous reactor and accelerator short baseline experiments. But again, in 1998 the Super-Kamiokande experiment [12] measured a significant asymmetry in up-down atmospheric neutrino muon events, indicating that they oscillate from a definite color to another through long distances.

Neutrino oscillations are of great theoretical and experimental interest, since observation of the phenomenon implies that the neutrino has non-zero mass, which was not included as part of the original SM. Neutrinos should have mass due to a mixture between the flavor and mass eigenstates. This means that the three neutrino physical states that interact with the charged leptons in weak interactions arise from a different superposition of the three neutrino states of definite mass [4].

2.4 Majorana neutrinos

After the observation of neutrino oscillations in atmospheric, solar, reactor and accelerator neutrino experiments a mechanism for the generation of neutrino masses was required, since the Standard Higgs mechanism can not explain it naturally. However, in 1937 E. Majorana theoretically demonstrated that all results of β-decay theory remain unchanged if the neutrino is its own anti-particle [4]. If the neutrinos turn out to be Majorana particles, they should manifest in lepton number violating processes where the total lepton number will be shifted by two units [13]. The light Majorana neutrinos have been searched in neutrinoless double beta decays of some nuclei [14]. On the other hand, $\Delta L = 2$ decays of pseudoscalar mesons [15] and tau leptons [16] have proven to be useful to constrain sterile neutrinos with masses in the MeV to a few GeV range (Figure 4.1) in different experiments.

2.5 Neutrinoless double beta decay

The discovery of neutrinoless double beta decay would represent a major breakthrough in particle physics. A single unequivocal observation of the decay would prove the Majorana nature of neutrinos and the violation of total lepton number. Unfortunately, this is by no means an easy task. The design of a detector capable of identifying efficiently and unambiguously such a rare signal poses a considerable experimental problem.

In double beta decay, two neutrons in the nucleus are converted to protons, and two electrons and two neutrinos are emitted. The process of neutrinoless double beta decay [17] denoted by $0\nu\beta\beta$ is described by the following decay equation

$$N_{A,Z} \rightarrow N_{A,Z+2} + 2e^{-} \tag{2.21}$$

and it is possible only if the neutrino and the antineutrino are actually the same particle. From this equation, it seems that $0\nu\beta\beta$ process doesn't conserve the leptonic number and for that reason it could not occur within the framework of the Standard Model. $0\nu\beta\beta$ process study was the first attempt to find *violation of leptonic number*, however until now the experiments haven't been able to find it [18].

In chapter 3 we discus the Belle II experiment and we discuss the possibility to find the leptonic number violation in chapter 4.

Chapter 3

Experimental setup

Besides of the neutrinoless double beta decay, there exists the possibility to find leptonic number violation at particle accelerators (also called colliders). These devices use electromagnetic fields to accelerate charged particles and then collide them. LCH [19] at CERN, RHIC [20] at Brookhaven National Laboratory, and Tevatron [21] at Fermilab, are some of these particle accelerators.

SuperKEKB [22] is the $e^+ e^-$ particle accelerator of asymmetric-energy that we used in this work as reference within its detector, *Belle II* [22]. The experiment is located at the High Energy Accelerator Research Organization in Tsukuba, Japan. This chapter briefly describes the SuperKEKB and Belle II setup and some differences with their predecessors, KEKB and Belle [23] , respectively.

3.1 SuperKEKB accelerator

SuperKEKB use the same two rings that were used by KEKB: a low-energy ring (LER) for positrons and a high-energy ring (HER) for electrons. These are located side by side 11 meters below the ground level in the TRISTAN tunnel, which has a circumference of around 3 km. However, the beam energies have been changed from the present values of 3.5 and 8.0 GeV to 4.0 and 7.0 GeV. In SuperKEKB the Nano-Beam scheme is used [22], where the idea is to minimize the longitudinal size of the overlap region of the two beams at the interaction point.

In the interaction region, the 7 GeV electrons in the HER and the 4 GeV positrons

in the LER collide at one interaction point (IP) with a non-zero crossing angle of 83 mrad.

3.2 Beam-induced background

In SuperKEKB, the expected luminosity will be 40 times higher than at KEKB [23], due to the higher beam currents and smaller interaction point beam sizes. These features will cause a higher beam-induced background in the Belle II detector. To assure stable detector operations at such high luminosity, an interaction region design based on beam background estimation is important.

The possible background sources are: synchrotron radiation (SR) from the HER upstream direction, it is important to evaluate and to protect the inner detectors (PXD and SVD); backscattering of SR from HER downstream, which is expected to produce much lower background than at KEKB; scattering of the beam on residual gas, this gas changes the momenta of beam particles, which then hit the walls of vacuum chambers and magnets ; Touscheck scattering, it is intra-bunch scattering and changes the momenta of beam particles in such a way that when they hit the vacuum chamber and magnet walls, shower particles are produced; radiative Bhabha scattering, which is proportional to the luminosity; and electron-positron pair production via the two photon process $e^+e^- \rightarrow e^+e^-e^+e^-$.

All these background are already considered for the Belle II detector, the details are described in [22].

3.3 Luminosity

The center-of-mass (CM) energy corresponds to the mass of the $\Upsilon(4S)$ resonance,

$$E_{CM} = 2\sqrt{E_{HER}E_{LER}} = 10.58GeV \sim M_{\Upsilon(4S)} \tag{3.1}$$

but at the interaction point, electrons and positrons undergo different types of interactions: Bhabha scatering, two-photon events, muon and tau pair production and quark pair production. Then, the production cross section for $\Upsilon(4S)$ (bound $b\bar{b}$ state) at the CM energy of 10.58 GeV is 1.1 nb, 1.3 nb for $c\bar{c}$ pair production, and

2.1 nb for $q\bar{q}$ pair production. Where q is a u, d, or s quark. Cross sections of various processes are summarized in Table 3.1.

Process	σ[nb]
$b\bar{b}$	1.1
$c\bar{c}$	1.3
$q\bar{q}$ $(q = u, d, s)$	2.1
$\tau^+\tau^-$	0.93
QED $(25.551° < \theta < 159.94°)$	37.8
$\gamma\gamma$	11.1

Table 3.1: Cross-section for various processes in e^+e^- collisions at $\sqrt{s} = 10.58$ GeV. QCD refers to Bhabha and radiative Bhabha processes.

The rate of interaction in e^+e^- collisions is proportional to the interaction cross section, $\sigma_{interaction}$:

$$\frac{dN_{\text{interaction}}}{dt} = \mathcal{L}_{e^+e^-}\sigma_{\text{interaction}} \tag{3.2}$$

where the coefficient $\mathcal{L}_{e^+e^-}$ is the luminosity of the accelerator and is a measure of the number of particles per unit area per unit time at the IP,

$$\mathcal{L}_{e^+e^-} = Fn\frac{N_{e^+}N_{e^-}}{A} \tag{3.3}$$

here, n is the number of bunches in the storage ring composed of N_{e^+} positrons and N_{e^-} electrons that collide F times per second and A is the overlapping area of the two colliding beams. The luminosity goal of SuperKEKB is $8 \times 10^{35}\text{cm}^{-2}\text{s}^{-1}$, which is around 50 times as large as the peak luminosity achieved by the KEKB collider.

3.4 Belle II Detector

For the Belle II detector, the main concern is to maintain the current performance of Belle in an environment with considerably higher background levels. In order to maintain a comparable or better performance than the Belle detector it was necessary its update. The updated features are listed below [22]:

- Just outside the beam pipe, the silicon strip detector is replaced by a two-layer silicon pixel detector based on the DEPFET (DEPleted Field Effect Transistor) technology;
- The silicon strip detector extends from just outside the pixel detector to a larger radius than in Belle;
- The readout of the silicon strip detector is based on the APV25 chip with a much shorter shaping time than the present readout based on the VA1TA chip;
- The central tracking device, a large volume drift chamber has smaller drift cells than in Belle, start just outside the expanded silicon strip detector, and extends to a larger radius;
- The completely new particle identification devices in the barrel and endcap region of the Cherenkov imaging type, with very fast readout electronics;
- The electronics of the electromagnetic calorimeter is of the wave-form-sampling type;
- The barrel part of the muon and K_L detector is equipped with RPCs, but with some inner layers, perhaps operating in proportional mode. While the endcap part is replaced with scintillators instrumented with silicon photomultipliers;
- The new data acquisition system meets the requirements of a considerably higher events rate.

In several aspects, Belle II will offer considerably better performance than Belle:

- The vertex resolution is improved by the excellent spatial resolution of the two innermost pixel detector layers;
- The efficiency for reconstructing K_S decays to two charged pions with hits in the silicon strip detector is improved because the silicon strip detector occupies a larger volume;
- The new particle identification devices in the barrel and endcap regions extend the very good pion/kaon separation to the kinematic limits of the experiment;

- The new electronics of the electromagnetic calorimeter considerably reduce the noise pile up, that is of particular importance for missing-energy studies.

Figure 3.1 shows the configuration of the Belle II detector, upgrade of the Belle detector. The detector is configured within a 1.5 T superconducting solenoid and iron structure surrounding the SuperKEKB beams. Decay vertices are reconstructed by a pixelated silicon sensors (PXD) and a silicon vertex detector (SVD), situated just outside a cylindrical beryllium beam-pipe. The main charged particle tracking is provided by a central drift chamber (CDC). Particle identification is provided by dE/dx measurements in the CDC and time-of-propagation (TOP) counters. Electromagnetic showers are detected in an array of CsI(Tl) crystals located inside the solenoid coil. Muon and K_L mesons are identified by arrays of resistive plate counters (RPCs) interspersed in the iron yoke.

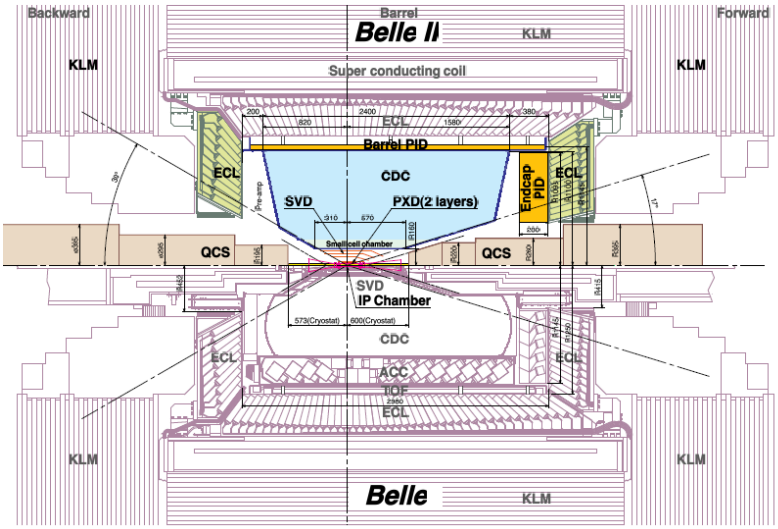

Figure 3.1: Upgrade Belle II spectrometer (top half) as compared to the Belle detector (bottom half).

The origin of the coordinate system is defined as the position of the nominal IP. The z axis is aligned with the direction opposite to the positron beam and is parallel to the direction of the magnetic field within the solenoid. The x axis is horizontal and points towards the outside of the ring, and the y axis is vertical. The polar angle θ and the azimuthal angle ϕ are measured relative to the positive z and x axes,

respectively. The radial distance is defined with $r = \sqrt{x^2 + y^2}$. The detector covers the polar angle θ from 17° to 150°, or about 93% of the solid angle.

The following subsections describe the Belle II subdetector modules. A complete description is given in Ref. [22]

3.4.1 Beam pipe

The Belle II detector will be precise in measurement of decay vertices. In order to reach this goal, the new silicon pixel detector should be placed as closed as possible to the IP and thus to the beam pipe wall. The beam pipe also needs to be as thin as possible in order to minimize the Coulomb scattering in the beam pipe wall, which can degrade the vertex resolution. An active cooling system is also needed for the beam pipe in order to remove the beam induced heat, which can reach a few hundred Watts.

The designed beam pipe has an inner radius of 10 mm, 10 μm Au, 0.6 mm Be, 1 mm coolant (paraffin) and 0.4 mm Be.

3.4.2 Pixel Detector (PXD)

At higher luminosities envisaged for SuperKEKB, the detectors close to the beam pipe are faced with extremely high hit rates, caused by beam-related background and by low-momentum-transfer QED processes. In the nano-beam option, the beam pipe radius in the interaction region will only be about 10 mm. This is good news for the vertex reconstruction, but is a challenge for the vertex detector itself because the background increases roughly with the inverse square of the radius. The innermost layers of a high precision vertex detector (in Belle detector) can no longer be realized by strip detectors due to the large occupancy, defined as the fraction of channels hit in each triggered event: the large strip occupancy at SuperKEKB luminosities makes the reconstruction of B-decay vertices impossible [23]. The solution is to use pixel sensors rather than strips for the innermost layers, which have a much larger number of channels and therefore a much smaller occupancy.

The PXD, see Fig. 3.2, based on the DEPFET technology, which allows for very thin (50 micron) sensors. In this concept, the readout electronics, which needs active

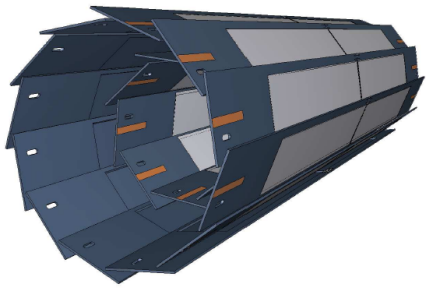

Figure 3.2: Schematic view of the geometrical arrangement of the sensors for the PXD.

cooling, are located outside the acceptance region and will therefore not contribute to the multiple-scattering material budget. The sensors themselves will consume very little power so that air cooling is sufficient. The PXD consist of two layers of sensors, with radii of 14 mm and 22 mm. The inner radius leaves sufficient space for possible variations of the final beam pipe layout.

3.4.3 Vertex Detector (SVD)

The main purpose of the Belle II SVD, together with the PXD and CDC is to measure the two B decay vertices for the measurement of mixing-induced CP asymmetry. In addition, the SVD measures vertex information in other decay channels, involving D-meson and τ-leptons decays.

The design of the Belle II SVD inherits the good characteristics of the Belle vertex detector: low mass, high precision, immunity to background hits, radiation tolerance and long-term stability. It is designed with silicon strip sensors to avoid the huge channel count of pixels without compromising the vertex-detection capability of Belle II.

Some characteristics of the Belle II SVD are the following:

- It improves the quality of the reconstruction of charged tracks compared to Belle's SVD2;
- It provides data to extrapolate the tracks reconstructed in the CDC to the PXD with high efficiency;

- The hit occupancy should be less than 10% in order to assure the association of correct hits in the vertex detector with tracks reconstructed in the drift chamber;
- In combination with the PXD, it is able to reconstruct low-p_t tracks, down to a few tens of MeV/c, that do not leave enough (or any) hits in the CDC. This is particularly important for the efficient reconstruction of the D^* daughters that tag the flavor of the parent B meson;
- It is able to reconstruct K_S mesons that decay outside of the PXD volume.

The Belle II SVD is composed of four layers, with sensor radii to 38, 80, 115, and 140 mm. The polar angular acceptance ranges from 17° to 150°, which is asymmetric to account for the forward boost of the center-of-mass frame, see Fig. 3.3. The radial coverage is almost double than that of the Belle SVD2 and hence would require a significantly increased number of wafers in a traditional cylindrical geometry.

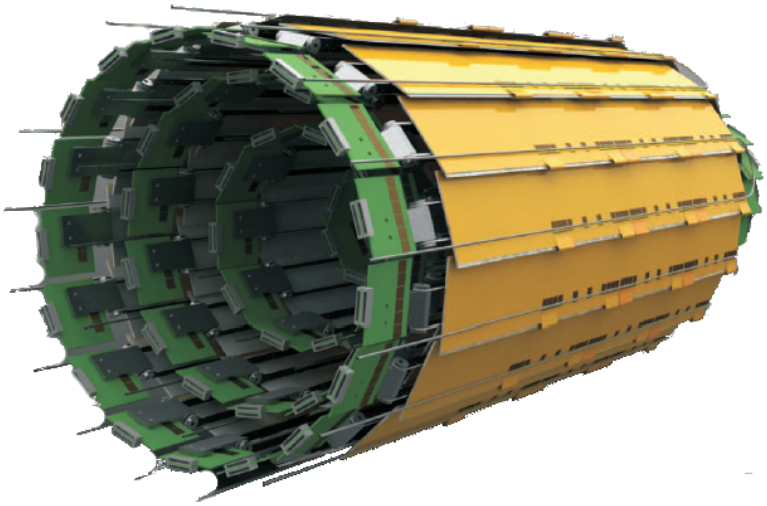

Figure 3.3: Belle II SVD barrel showing all four layers, cooling lines and hybrids.

3.4.4 Central Drift Chamber (CDC)

In the Belle II detector, the central drift chamber (CDC) plays three important roles. First, it reconstructs charged tracks and measures their momenta precisely.

Second, it provides particle identification information using measurements of energy loss within its gas volume. Low-momentum tracks, which do not reach the particle identification device, can be identified using the CDC alone. Finally, it provides efficient and reliable trigger signals for charged particles.

The Belle CDC has worked well for more than ten years without any serious problems. Therefore, the Belle II CDC follows the global structure of its predecessor for the material of the major parts, the superlayer wire configuration, the cell structure, the wire material, and the gas mixture. The main parameters are listed in Table 3.2, together with those of the Belle CDC for comparison. The main differences between both designs are:

- First, the new readout electronics system must handle higher trigger rates with less deadtime;
- Second, to avoid the high-radiation and high-background region near the interaction point and to provide more space for the SuperSVD, the CDC inner radius is 160 mm. Since the Belle II barrel particle identification device is more compact than in Belle, the CDC outer radius is 1130 mm. A new wire configuration fills the modified volume;
- Third, the CDC generates three-dimensional trigger information. A z trigger for charged particles is essential to reduce background without sacrificing physics events.

	Belle	Belle II
Radius of inner cylinder (mm)	77	160
Radius of outer cylinder (mm)	880	1130
Radius of innermost sense wire (mm)	88	168
Radius of outermost sense wire (mm)	863	1111.4
Number of layers	50	56
Number of sense wires	8400	14336
Gas	He-C_2H_6	He-C_2H_6
Diameter of sense wire (μm)	30	30

Table 3.2: Main parameters of the Belle CDC and the CDC upgrade for Belle II.

3.4.5 Particle Identification - Barrel

To improve the K/π separation capability of the spectrometer it is needed to upgrade the particle identification (PID) system. In the barrel region of the spectrometer, the present time-of-flight and the aerogel Cherenkov counters are replaced with a time-of-propagation (TOP) counter [24]. In this counter, the time of propagation of the Cherenkov photons internally reflected inside a quartz radiator is measured, as shown in Fig. 3.4. The Cherenkov image is reconstructed from the 3-dimensional information provided by two coordinated (x, y) and precise timing, which is determined by micro-channel plate (MCP) photomultipliers tubes (PMTs) at the end surfaces of the quartz bar. The array of quartz bars, surrounds the outer wall of the CDC; they are divided into 16 modules in ϕ in the baseline geometry.

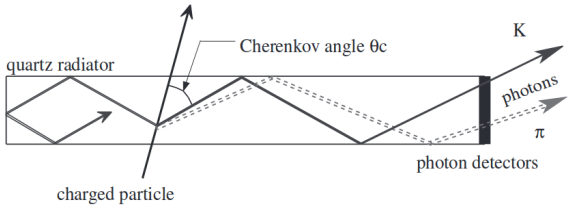

Figure 3.4: Schematic side view of TOP counter and internal reflecting Cherenkov photons.

3.4.6 Particle Identification: End-cap

Identification of charged particles over the full kinematic range is one of the basic requirements for Belle II. In the forward endcap, the proximity-focusing Aerogel Ring-Imaging Cherenkov detector (ARICH) has been designed to separate kaons from pions over most of their momentum spectrum and to provide discrimination between pions, muons and electrons below 1 GeV/c.

Fig. 3.5 shows the ARICH elements, which are:

- An aerogel radiator where Cherenkov photons are produced by charged particles,
- An expansion volume to allow Cherenkov photons to form rings on the photons detector surface,

- An array of position sensitive photon detectors, that is capable of detecting single photons in a high magnetic field with high efficiency and with good resolution in two dimensions, and
- A readout system for the photon detector.

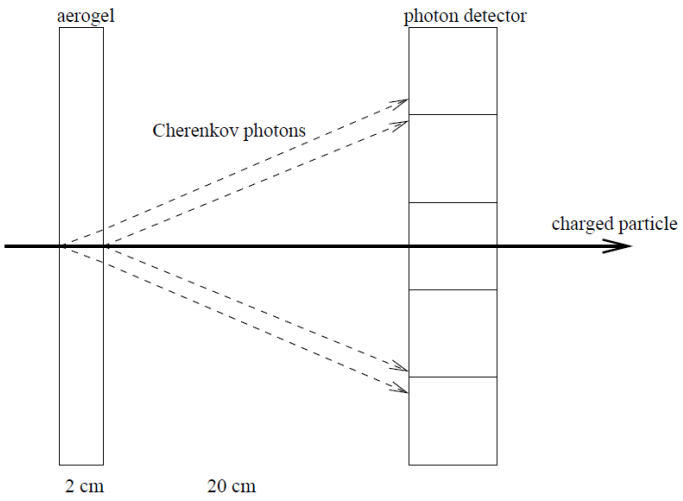

Figure 3.5: ARICH principle.

3.4.7 Electromagnetic Calorimeter (ECL)

CsI(Tl) was chosen as the scintillation crystal material for the Belle calorimeter due to its high light output, relatively short radiation length, good mechanical properties and moderate price. The main tasks of the calorimeter are:

- Detection of photons with high efficiency,
- Precise determination of the photon energy and angular coordinates,
- Electron identification,
- Generation of the proper signal for trigger,
- On-line and off-line luminosity measurement, and

- K_L^0 detection together with the KLM.

The Belle electromagnetic calorimeter (ECL) consists of a 3 m long barrel section with an inner radius of 1.25 m and annular endcaps at $z = 1.96$ m and $z = -1.02$ m from the interaction point. The calorimeter covers the polar angle region of $12.4° < \theta < 155.1°$, except for the two gaps $\sim 1°$ wide between the barrel and endcaps. The barrel part has a tower structure that projects in a region near the vicinity of the interaction point. It contains 6624 CsI(Tl) crystals of 29 distinct shapes. Each crystal is a truncated pyramid of an average size about $6 \times 6\text{cm}^{-2}$ in cross section and 30 cm (16.1 X_0) in length. The endcaps consists of 2112 CsI crystals of 69 shapes. The total number of crystals is 8736, with a total mass of about 43 tons.

The Belle detector has been operating since 1999 and, throughout this period, the calorimeter has demonstrated high resolution and good performance. However, the Belle II experiment, operating with a luminosity of up to $8 \times 10^3 5\text{cm}^{-2}\text{s}^{-1}$, puts several requirements on the calorimeter which are considered in the upgrade.

3.4.8 K_L^0 and μ detection (KLM)

The K_L and muon detector (KLM), shown in Fig 3.1, consists of an alternating sandwich of 4.7 cm thick iron plates and active detector elements located outside the superconducting solenoid. The iron plates serve as the magnetic flux return for the solenoid. They also provided 3.9 interaction lengths or more of matter, beyond the 0.8 interaction lengths of the calorimeter, in which K_L mesons can shower hadronically.

The octagonal barrel covers the polar angle range from 45° to 125°, while the endcaps extend this coverage from 20° to 155°. There are 15 detector layers and 14 iron plates in the barrel and 14 detector layers and 14 iron plates in each endcap. Muons and non-showering charged hadrons with a momentum above ~ 0.6 GeV/c traverse the KLM until they escape or range out due to electromagnetic energy deposition. K_L mesons that interact in the ECL or the iron plates create a hadronic shower that can be detected in either the ECL alone, the KLM alone, or both.

3.5 Software Framework

BASF (Belle Analysis Framework), the software framework used successfully at Belle require modifications of nearly all parts of the software due to the upgrade and the new incorporated detectors. The new software framework, called **basf2** [25], incorporates concepts of other experiments into its design, but primarily follows concepts proven in BASF. The architecture of basf2 is modular, in which all processing method is encapsulated within a module, with multiple modules arranged in a strict linear order inside a container called a path. The user can create an arbitrary number of modules and paths with one or more paths linked together to form a data processing chain. A simple example of a path consisting of 4 modules is in the figure 3.6. The tasks of the modules vary from simple ones, such as reading data from a file, to complex tasks, such as full detector simulation described below.

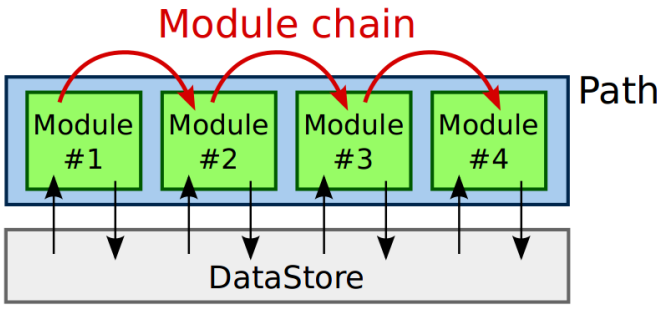

Figure 3.6: A simple data processing chain. One path containing 4 modules that exchange data with each other using the common DataStore.

The modules are executed one at a time, exactly in the order in which they were placed into the path and all modules in the path share the DataStore module.

The simulation of possible events in Belle II detector is the first objective of **basf2**, the theory is applied in each step of the process (Figure 3.7), the real collisions are substituted by Monte Carlo simulation generators. Some of these generators are **EvtGen** [26] for **B** mesons and **KKMC** [27] for the τ's, both using the expected conditions in the experiment to produce these particles.

The geometry and properties of each subdetector mentioned in the section 3.4 are created by **Geant4** [28] and it is the second step in the process of the collision.

Here, the properties of the generated particle are stored but also we have information about all particles, so we can identify them. Finally, we used the same reconstruction algorithms that will be used with the real data and the tools provided by **ROOT** [29], all described in the next sections.

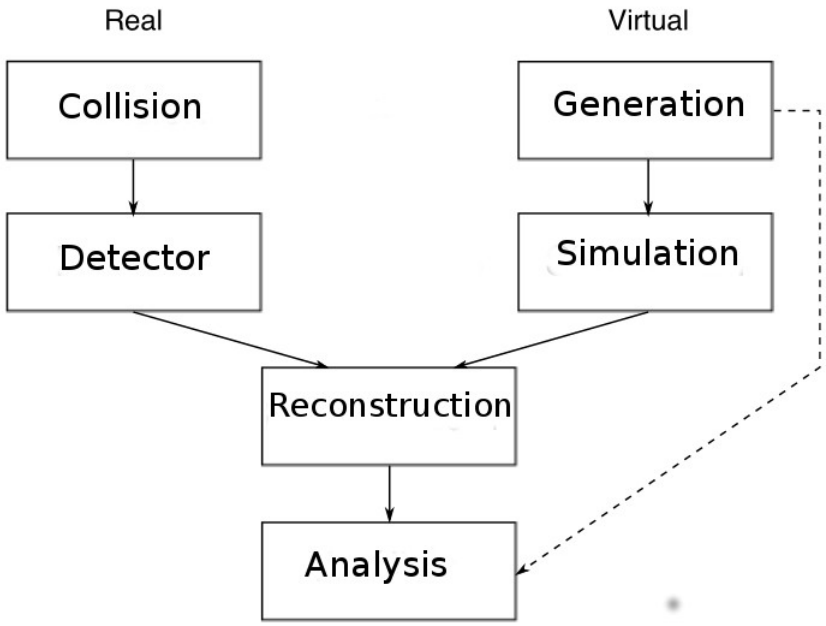

Figure 3.7: Functionality of basf2 with respect to real collision events.

3.5.1 Generation

Monte Carlo generators in high energy physics provide simulations of particle collisions. They play an essential role in data analysis, where they are used together with detector simulation to provide a realistic estimate of the detector response to collision events. In this work, we used the generator **KKMC** [27][30][31] that is included in basf2. KKMC generates $ee \to \mu\mu(\gamma)$ and $ee \to \tau\tau(\gamma)$, the KKMC4.19 version includes next to leading order (NLO) corrections to initial state radiation (ISR) and final state radiation (FSR), final state masses are taken into account also for higher order QED corrections but the electron masses are neglected apart from kinematics effects. τ decays within KKMC are handled by the TAUOLA [32] or

PYTHIA [33] package and radiative correction to τ decays are included using the PHOTOS package.

The scripts used in this work have the next form

PDG	Tau pair		3Q	2h	NColor	mass	aux.parm.	lifetime	decay	Jetset parm.
15	tau-	tau+	-3	0	1	1.77	0.000	0.000	8.71E-2	0 1
dec.opt.	GEN	BR	decay channel PDG							
1	2101	0.1785	-12	11	16	0	0			
2	2102	0.1736	-14	13	16	0	0			
3	41	0.0001	16	-321	221	0	0			

Here, the first row is always the same due to the experiment and we have the PDG number of the τ (15), the τ pair production (tau+ tau-), three times their charge (3(-1)), two times their helicity (2(0)), NColor (1 for all leptons), mass (1.777 MeV), auxiliary parameters (0 0), life time (8.71100E-02), 1(0) to decay (don't decay) τ's, and 1(0) to (don't) use Jetset.

The next rows are different, here we can write all channels we want, for instance, in the third row we have $\tau^- \to e^- + \bar{\nu}_e + \nu_\tau$. In the first column we have the decay options (1, 2 or 3) where 1 means both tau+/tau-, 2 means tau-, and 3 tau+; in the second column when it set more than 2000 the decay is simulated by TAUOLA, in other cases, PYTHIA does. In the next columns there are PID of the particles we want.

3.5.2 Geometry

Geant4 [28], a tool for the simulation of the passage of particles through matter, is used to construct all Belle II sub-detectors (Figure 3.8) described in section 3.4. Then, the generated particles by KKMC will be propagated through the Belle II detector and their information will be stored. This information is about the deposited energy in each detector, the number of activated clusters, the momentum of the particles, and others variables. To identify the particle at all time, is the principal advantage of this tool. This information is more than what we will obtain in real experiment, so we can select different types of information. This selection of information will allow us to simulate the real data produced by the Belle II experiment

in the next years.

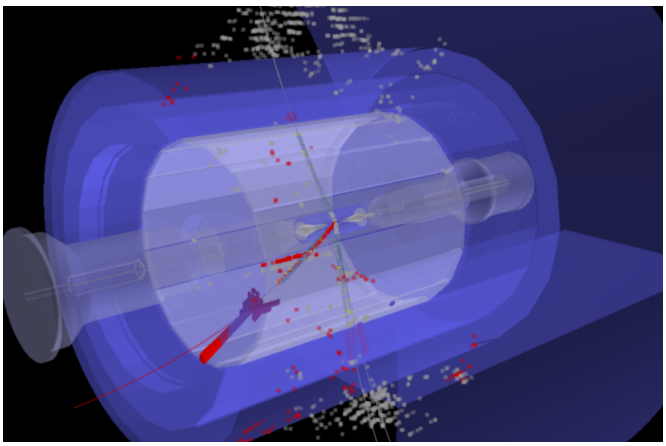

Figure 3.8: Event simulated in Geant4.

3.5.3 Analysis

To understand the physic of the simulated or real collision events it is necessary to observe their distributions in several variables. In simulated events these distributions depend of the used models by the generators and with real events we can match them and select the best model. We can manage this distributions with **ROOT** [29], a specialized software in particle physics, which provides the tools necessary to manage large amounts of data. ROOT is based in the programming language C++, which allows us to organize the information in trees (their basic structures) and represent it through histograms.

Chapter 4

Analysis and results

The decay studied in this work is

$$\tau^- \rightarrow \pi^+ \mu^- \mu^- \nu_\tau \tag{4.1}$$

which violates the leptonic number by two units ($\Delta L = 2$). As mentioned in **section 2.4**, the experimental observation of decays in which $\Delta L = 2$ allows us to know the nature of Majorana neutrinos. Searches on three bodies decays to three bodies have been done by different experiments [6], see Fig. 4.1.

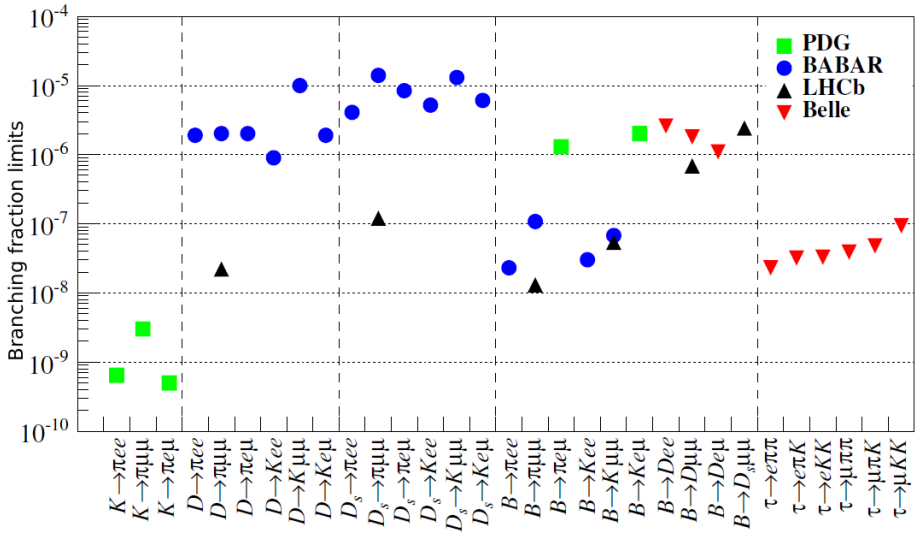

Figure 4.1: Branching fraction limits in channels where $\Delta L = 2$.

But non decay process have been observed experimentally and limits in branching fractions have been imposed. The Majorana neutrino mass (m_N) in the range of $\sim$ (100 GeV - 1 TeV) can explain the suppressed channels. However, the m_N is not determined and other cases can exist. In particular, when m_N in the range of $\sim$(MeV to few GeV) the branching fractions can be enhanced for decays to four bodies (for more details see [6]). We focus in semi-leptonic decays (Figure 4.2) where we can observe the branching fraction to $\tau^- \rightarrow \pi^+\mu^-\mu^-\nu_\tau$ channel, the most accessible channel. We will study the possibility to find this channel in the Belle II detector.

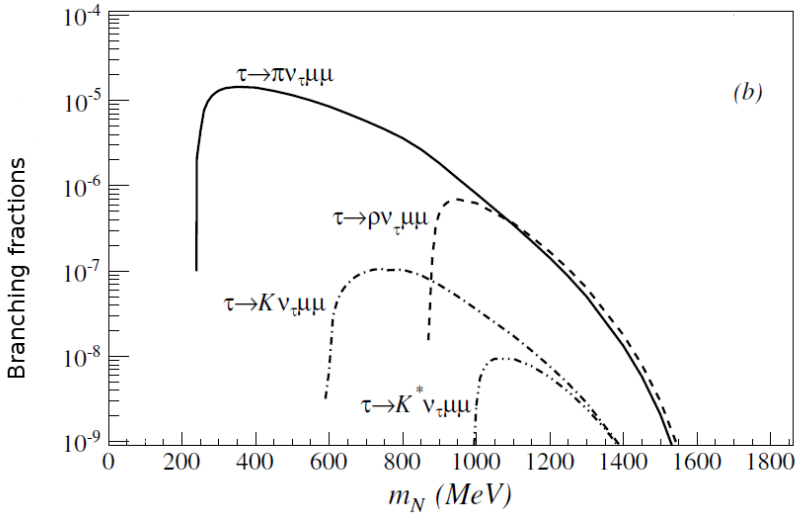

Figure 4.2: Branching fraction limits in which $\Delta L = 2$. Lepton decays to four bodies.

These decay processes violate the total lepton number by two units and can be induced by the exchange of Majorana neutrinos. We consider a scenario where these decays are dominated by the exchange of only one heavy neutrino, which produces an enhancement of the decay amplitude via the resonant mechanism and the high luminosity in the Belle II experiment to study the $\tau^- \rightarrow \pi^+\mu^-\mu^-\nu_\tau$ channel.

4.1 Simulation

In real collisions the particles are produced arbitrarily, but here, we have the control of the produced particles. We are interested in the $\tau^- \rightarrow \pi^+\mu^-\mu^-\nu_\tau$ channel. Then,

we called it **signal**. However, there are a lot of channels that could occur. We select the channels which are similar to the signal channel but they don't violate the leptonic number. We called them **background**.

- Signal

  $\tau^- \to \pi^+\mu^-\mu^-\nu_\tau$, (BR $\lesssim 10^{-5}\%$) [6]

- Background

  $\tau^- \to \pi^+\mu^-\mu^+\nu_\tau$, (BR $\sim 10^{-6}\%$) [34]

  $\tau^- \to \pi^+\pi^-\pi^-\nu_\tau$, (BR $9.31 \pm 0.06\%$) [34]

We will compare the background to signal events in order to know the possibility to find and differentiate the signal channel from the background in the real data of Belle II experiment. In general we used a set of variables and constructed their distributions, then we applied different cuts to select the best constraints, first for the invariant mass window, then for the particle identification (PID) for π's and μ's, and finally for the beam constrained mass.

The analysis was done in **ROOT** and is shown below, where we considered the next observable distributions:

- Transverse momentum, p_t
- Pseudorapidity, η
- Polar angle, θ

We selected these variables since they are most general in high energy physics and some of the most used in the literature.

Up to this day the experiment have not started and all data in this work have been simulated (see section 3.5). 50,000 events were generated by **KKMC** for each channel. Furthermore, the information provided by **basf2** (Section 3.5) is more than that we will obtain in the real experiment. In order to have an approximation to real experiment or real data we use two set of variables. First, the information about the reconstructed events by the Belle II algorithms that we called **Reconstruction**

data. Here, we only have hits in the sub-detectors of Belle II and we reconstruct the traces of the possible particles. Second, in addition to the above information we use the information of the generated events by KKMC to match the events which are well reconstructed. Here, we called them **Simulation data**.

- Simulation data: {Four momentum; Invariant mass of the particles; **PDG code of matched MCParticles**; Pion and Muon ID probability; Beam constrained mass (Mbc)}
- Reconstruction data: {Four momentum; Invariant mass of the particles; Pion and Muon ID probability; Beam constrained mass (Mbc)}

In the next sections it is described the used method in this work.

4.1.1 Mass cut

The produced particles were propagated through the Belle II detector using **Geant4**. And finally the particles were reconstructed with Belle II algorithms, but in this step some events cannot be reconstructed for different reasons. For instance, if the particles are outside of the Belle II detector, or its efficiency is insufficient, or the algorithms used fail. Furthermore, each channel has at least one neutrino, this means loss of energy. Then the first choice would be to reconsider the invariant mass window we need. We want to reconstruct τ's with invariant mass of 1.776 GeV, then the invariant mass windows are (these figures only contain the signal channel):

- $1.0 < M_\tau < 1.9$ GeV (Figure 4.3)
- $1.3 < M_\tau < 1.9$ GeV (Figure 4.4)
- $1.5 < M_\tau < 1.9$ GeV (Figure 4.5)

The amount of reconstructed and simulated events for each channel and for each invariant mass window is shown in **Table 4.1**.

In the Table 4.1 we can see the amount of events reconstructed and we would expect almost 50,000 events (generated events). However, the only case with this

amount is $1.0 < M < 1.9$ GeV for the signal. We can neglect the $1.5 < M < 1.9$ GeV case due to its low amount of events.

Channel	$1.0 < M < 1.9$ GeV		$1.3 < M < 1.9$ GeV		$1.5 < M < 1.9$ GeV	
	recons	sim	recons	sim	recons	sim
$\tau^- \to \pi^+\mu^-\mu^-\nu_\tau$	53,192	28,429	31,275	14,419	16,036	4,845
$\tau^- \to \pi^+\mu^-\mu^+\nu_\tau$	94,495	28,657	54,084	14,515	26,206	4,925
$\tau^- \to \pi^+\pi^-\pi^-\nu_\tau$	83,515	33,454	49,679	17,513	26,611	6,339

Table 4.1: Reconstructed and simulated events for each channel, only mass cut is used.

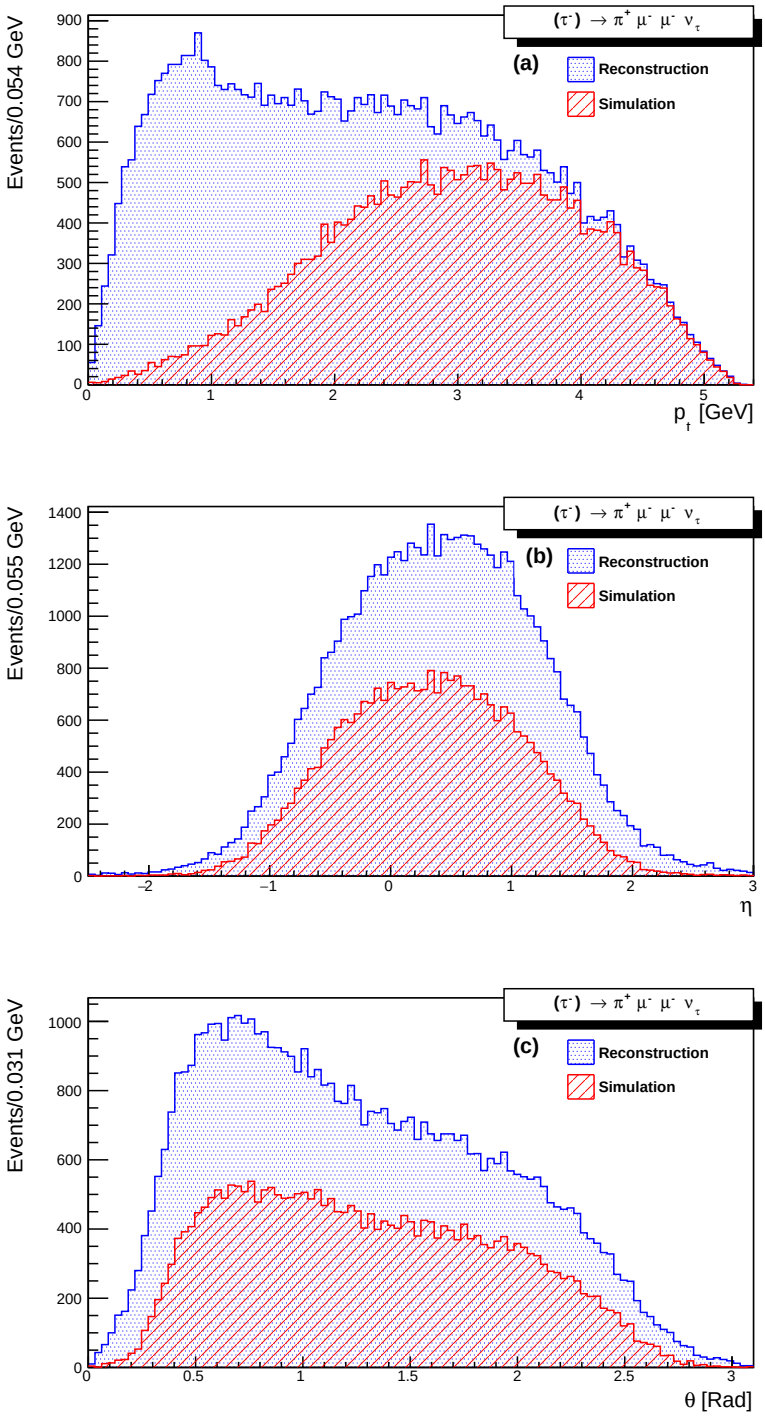

Figure 4.3: Transerve momentum (top), pseudorapidity (middle) and polar angle (bottom). Invariant mass with a window of $1.0 < M_\tau < 1.9$ GeV for the channel $\tau^- \to \pi^+\mu^-\mu^-\nu_\tau$, using 53,192 reconstructed events and 28,429 simulated events.

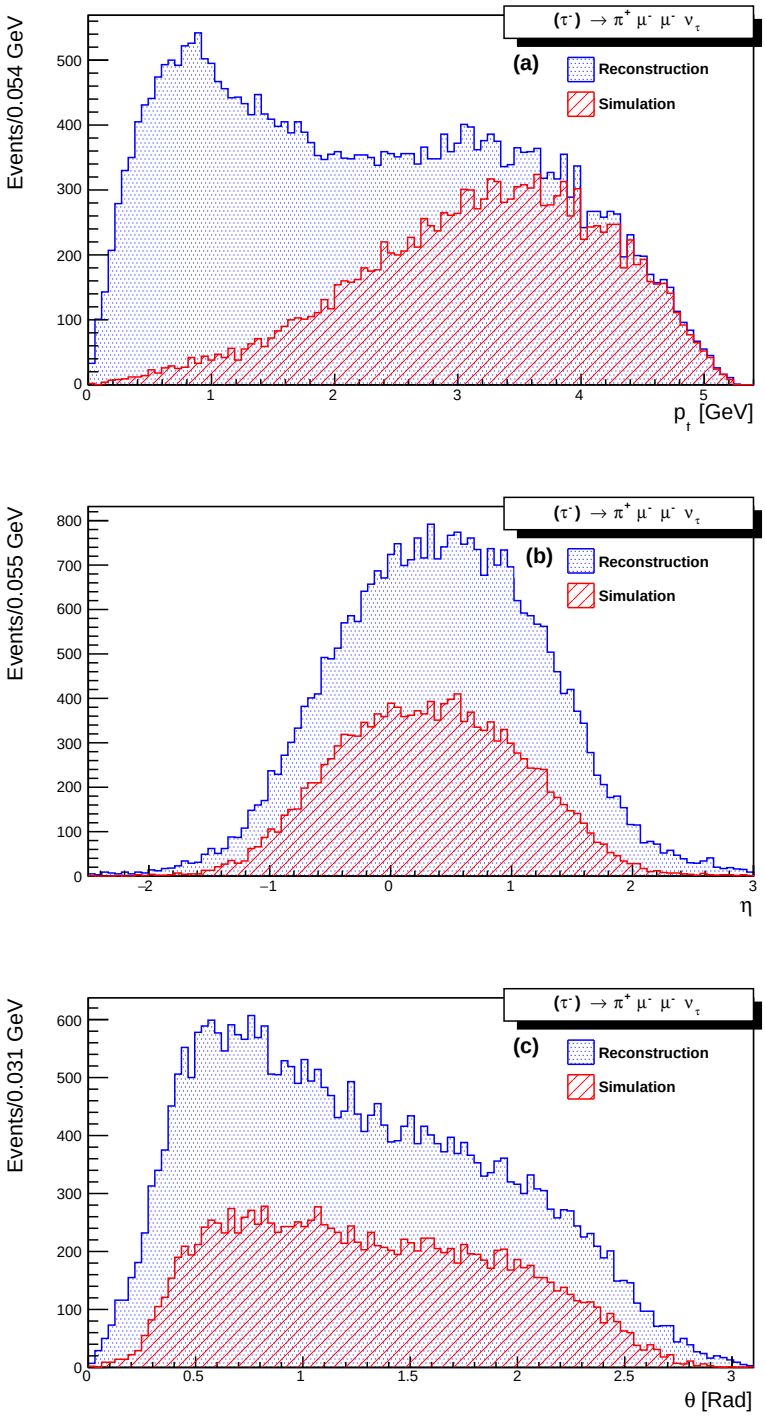

Figure 4.4: Transerve momentum (top), pseudorapidity (middle) and polar angle (bottom). Invariant mass with a window of $1.3 < M_\tau < 1.9$ GeV for the channel $\tau^- \to \pi^+\mu^-\mu^-\nu_\tau$, using 31,275 reconstructed events and 14,419 simulated events.

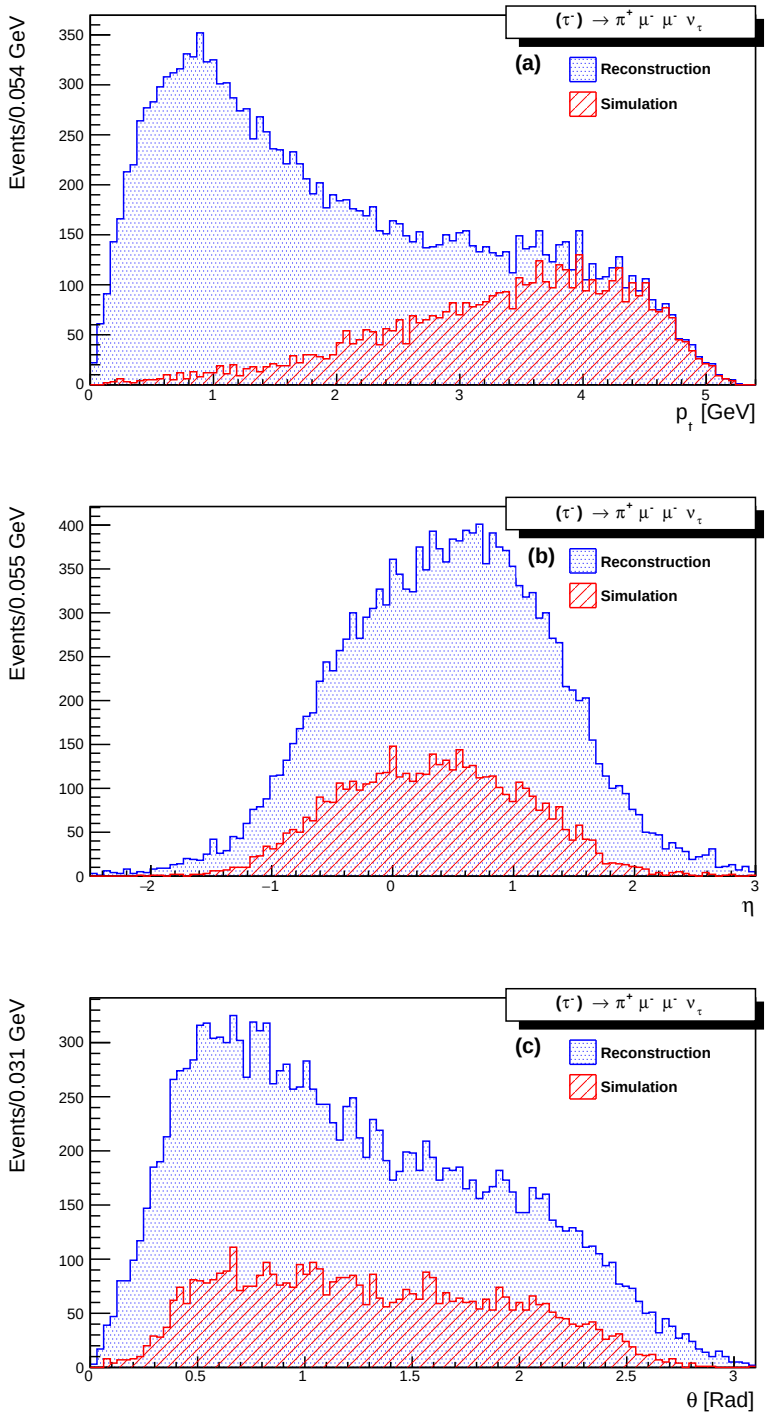

Figure 4.5: Transerve momentum (top), pseudorapidity (middle) and polar angle (bottom). Invariant mass with a window of $1.5 < M_\tau < 1.9$ GeV for the channel $\tau^- \to \pi^+\mu^-\mu^-\nu_\tau$, using 16,036 reconstructed events and 4,856 simulated events.

4.1.2 Detector efficiency

Now, we consider the detector efficiency, especially for π and μ identification. Belle II detector will be pretty efficient in particle identification (PID), however the energy loss due to the neutrinos is necessary. In this work such variable is not considered to reconstruct the τ's, for this reasons we used arbitrary values: 80% > for π's and two values for μ's 20% > and 40% >. **Table 4.2** shows the results with μ's at 20% > and 40% > identification, and the Fig. 4.6 to 4.8 shown the observable distributions (again only signal channel for the figures):

Channel	$1.0 < M < 1.9$ GeV				$1.3 < M < 1.9$ GeV			
PID $\mu \geq$	20%		40%		20%		40%	
	recons	sim	recons	sim	recons	sim	recons	sim
$\tau^- \to \pi^+\mu^-\mu^-\nu_\tau$	27,258	20,789	24,119	18,864	14,879	10,584	13,196	9,681
$\tau^- \to \pi^+\mu^-\mu^+\nu_\tau$	38,330	20,883	32,848	19,064	21,184	10,663	18,226	9,787
$\tau^- \to \pi^+\pi^-\pi^-\nu_\tau$	45,109	22,959			26,363	11,713		

Table 4.2: Reconstructed events for each channel, with two PID cuts.

In the Table 4.2 we can see that the amount of events reconstructed decreases significantly from 20% to 40% and both cases $1.0 < M < 1.9$ GeV and $1.3 < M < 1.9$ GeV. On the other hand distribution shapes of invariant mass cuts and particle identification are very similar. If we observe the simulation distributions in all transverse momentum distributions, the particles with low momentum could be considered as poorly reconstructed. Furthermore, we need to conserve the most amount of simulated particles. Then, we continue exclusive only particle identification of μ's at 20% > and $1.0 < M < 1.9$ GeV case.

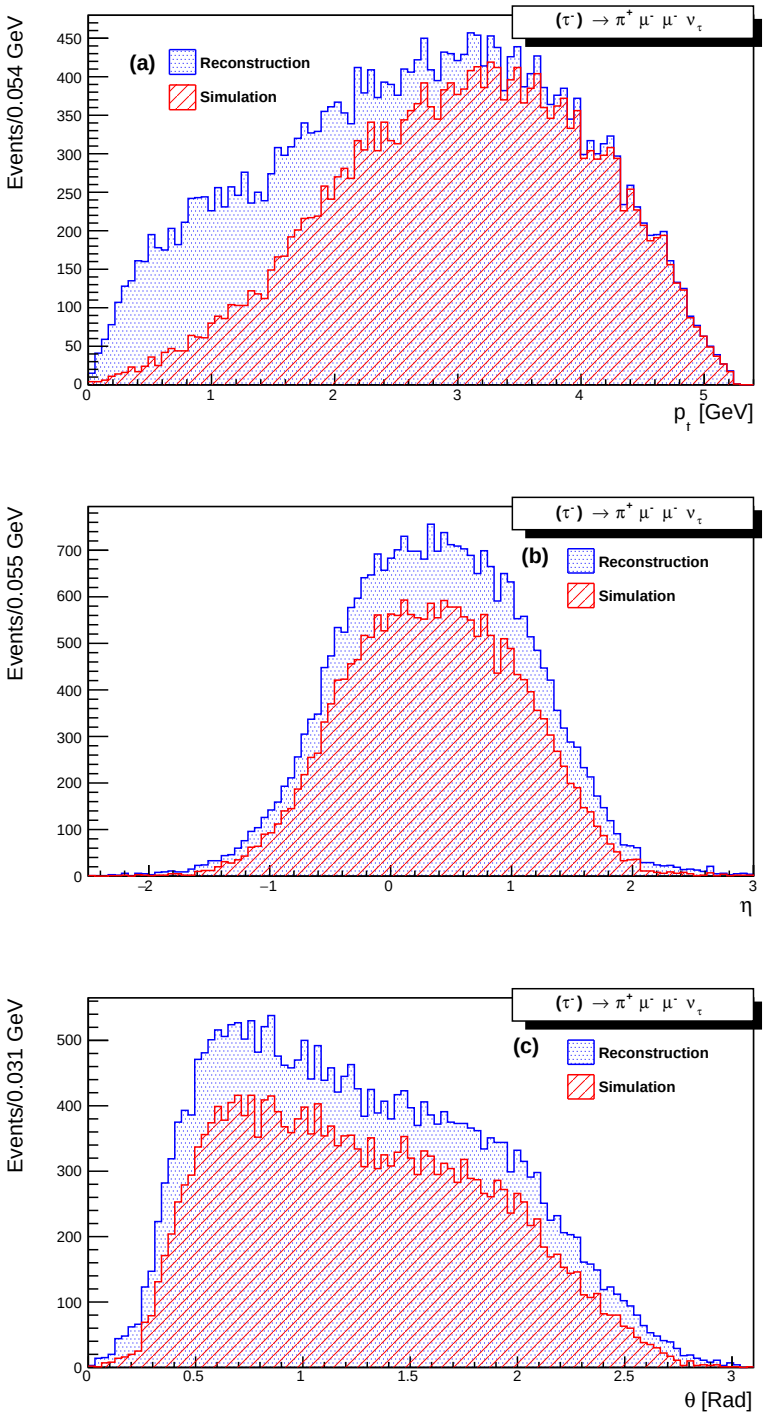

Figure 4.6: Transerve momentum (top), pseudorapidity (middle) and polar angle (bottom) for the decay channel $\tau^- \to \pi^+\mu^-\mu^-\nu_\tau$ with an invariant mass window of $1.0 < M_\tau < 1.9$ GeV, PID ($\mu > 20\%$ $\pi > 80\%$), using 27,258 reconstructed events (blue) and 20,789 simulated events (red).

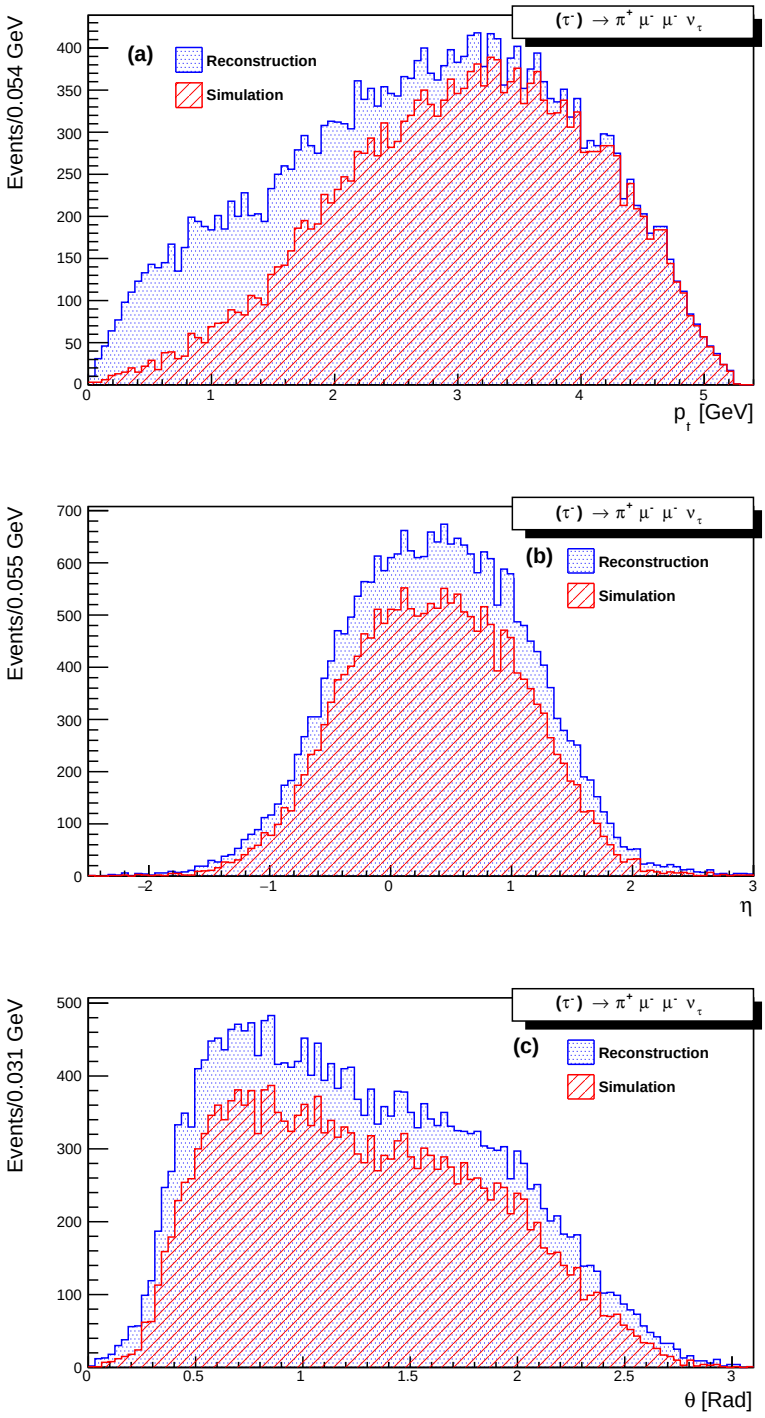

Figure 4.7: Transerve momentum (top), pseudorapidity (middle) and polar angle (bottom) for the decay channel $\tau^- \to \pi^+\mu^-\mu^-\nu_\tau$ with an invariant mass window of $1.0 < M_\tau < 1.9$ GeV, PID ($\mu > 40\%$ $\pi > 80\%$), using 24,119 reconstructed events (blue) and 18,864 simulated events (red).

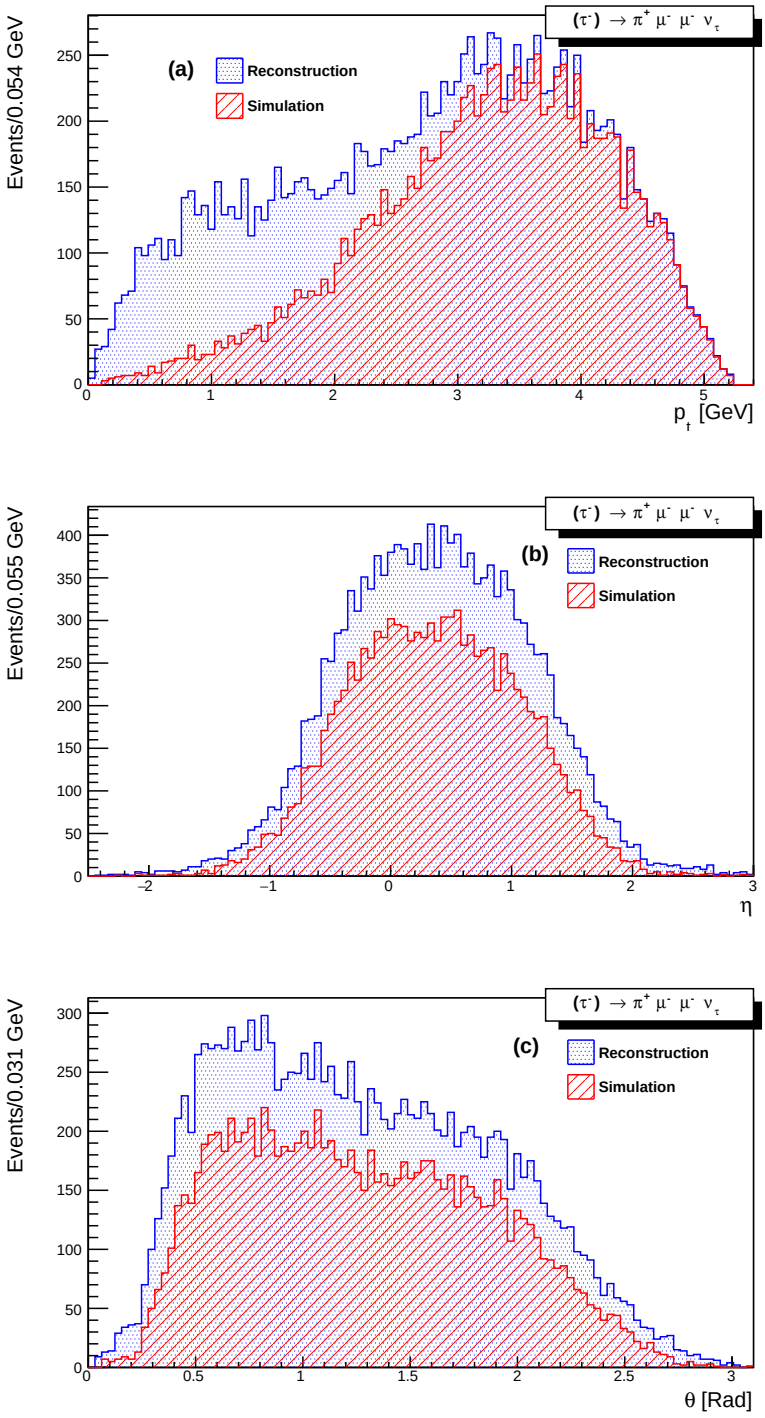

Figure 4.8: Transerve momentum (top), pseudorapidity (middle) and polar angle (bottom) for the decay channel $\tau^- \to \pi^+\mu^-\mu^-\nu_\tau$ with an invariant mass window of $1.3 < M_\tau < 1.9$ GeV, PID ($\mu > 20\%$, $\pi > 80\%$), using 14,879 reconstructed events (blue) and 10,584 simulated events (red).

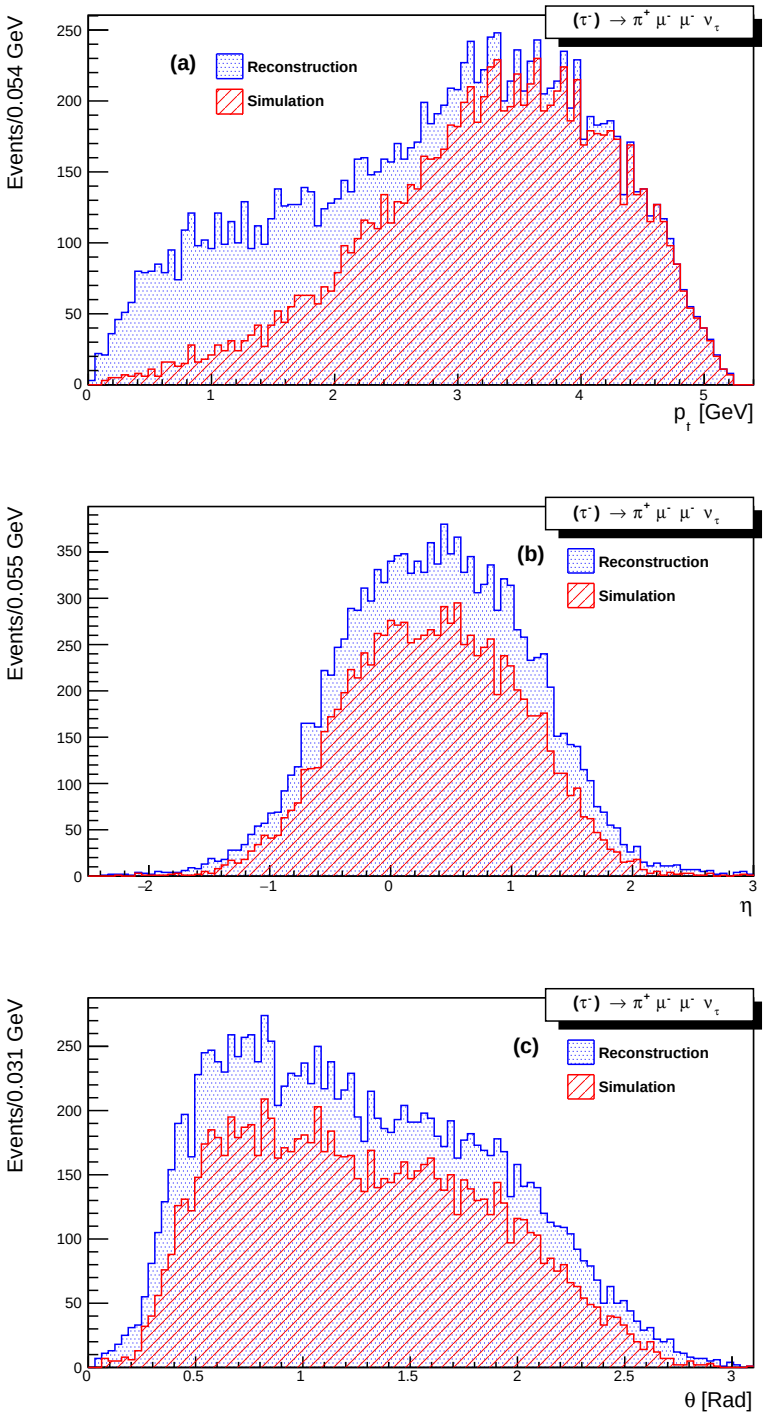

Figure 4.9: Transerve momentum (top), pseudorapidity (middle) and polar angle (bottom) for the decay channel $\tau^- \to \pi^+\mu^-\mu^-\nu_\tau$ with an invariant mass window of $1.3 < M_\tau < 1.9$ GeV, PID ($\mu > 40\%$, $\pi > 80\%$), using 13,196 reconstructed events (blue) and 9,681 simulated events (red).

4.1.3 Beam constrained mass

The conventional method for observing resonant signals in particle physics analysis is by the selecting a set of tracks and studying the invariant mass (M_{inv}):

$$M_{inv} = \sqrt{\left(\sum_i E_i^2\right)^2 - \left(\sum_i \vec{p_i}\right)^2} \tag{4.2}$$

where E and $\vec{p})_i$ are the energy and three-momentum of track i, respectively. But we are considering channels with at least one neutrino. Then, the resolution of the invariant mass is 1.0 to 1.9 GeV. Improvements can be obtained if we consider that the τ pair is produced at the rest frame where each τ is produced with an energy equal to that of the beam in the laboratory frame. We replace the energy of the τ with the energy of the beam in the equation (4.2). The resulting equation is called the beam constrained mass (M_{bc}):

$$M_{bc} = \sqrt{E_{beam}^2 - \left(\sum_i \vec{p_i}\right)^2} = \sqrt{E_{beam}^2 - p_\tau^2} \tag{4.3}$$

where E_{beam} and $\vec{p_i}$ are half of the beam energy and momentum of produced particles, respectively. The beam constrained mass only consider primary particles, in these case τ particles. This variable is important due to the fact that the total energy is sensitive to the mass hypotheses made on the decay products, while the beam constrained mass quantity requires that they have the correct momentum. Another advantage of having a second independent mass variable lies in the reduction of background from missidentification, here neutrinos.

Channel	$1.0 < M < 1.9$ and $M_{bc} \leq 4$GeV	
	recons	sim
$\tau^- \to \pi^+\mu^-\mu^-\nu_\tau$	11,991	11,680
$\tau^- \to \pi^+\mu^-\mu^+\nu_\tau$	13,208	10,834
$\tau^- \to \pi^+\pi^-\pi^-\nu_\tau$	11,812	11,116

Table 4.3: Reconstructed events; mass, PID and M_{bc} cuts are used.

In figures 4.10 to 4.12, we can observe the influence of M_{bc} variable with respect

to the observable distribution, especially in $\tau^- \to \pi^+\mu^-\mu^-\nu_\tau$ and $\tau^- \to \pi^+\pi^-\pi^-\nu_\tau$ channels, however the $\tau^- \to \pi^+\mu^-\mu^+\nu_\tau$ channel is poorly reconstructed yet.

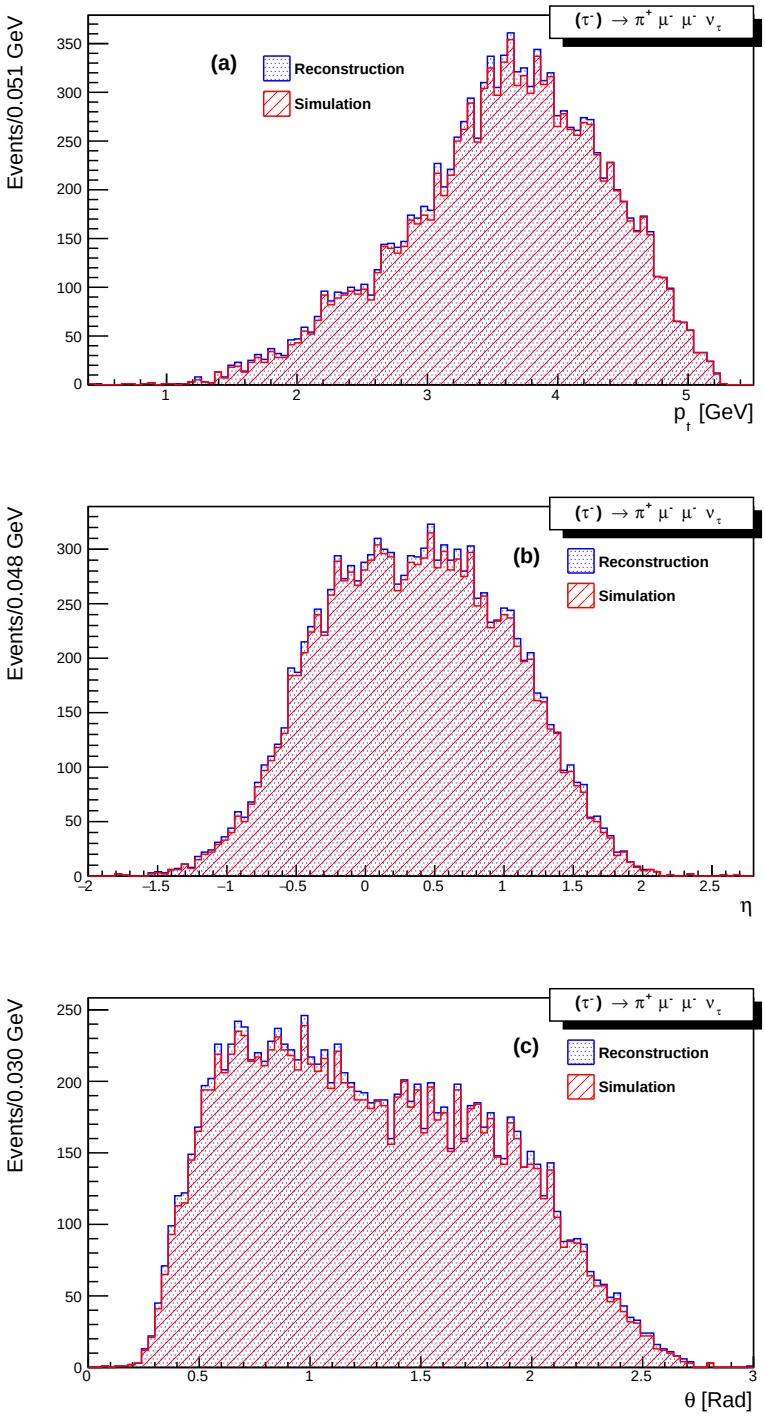

Figure 4.10: Transerve momentum (top), pseudorapidity (middle) and polar angle (bottom) for the decay channel $\tau^- \to \pi^+\mu^-\mu^-\nu_\tau$ with an invariant mass window of $1.0 < M_\tau < 1.9$ GeV, PID ($\mu > 20\%$ $\pi > 80\%$), $M_{bc} \leq 4$ GeV, using 11,991 reconstructed events (blue) and 11,680 simulated events (red).

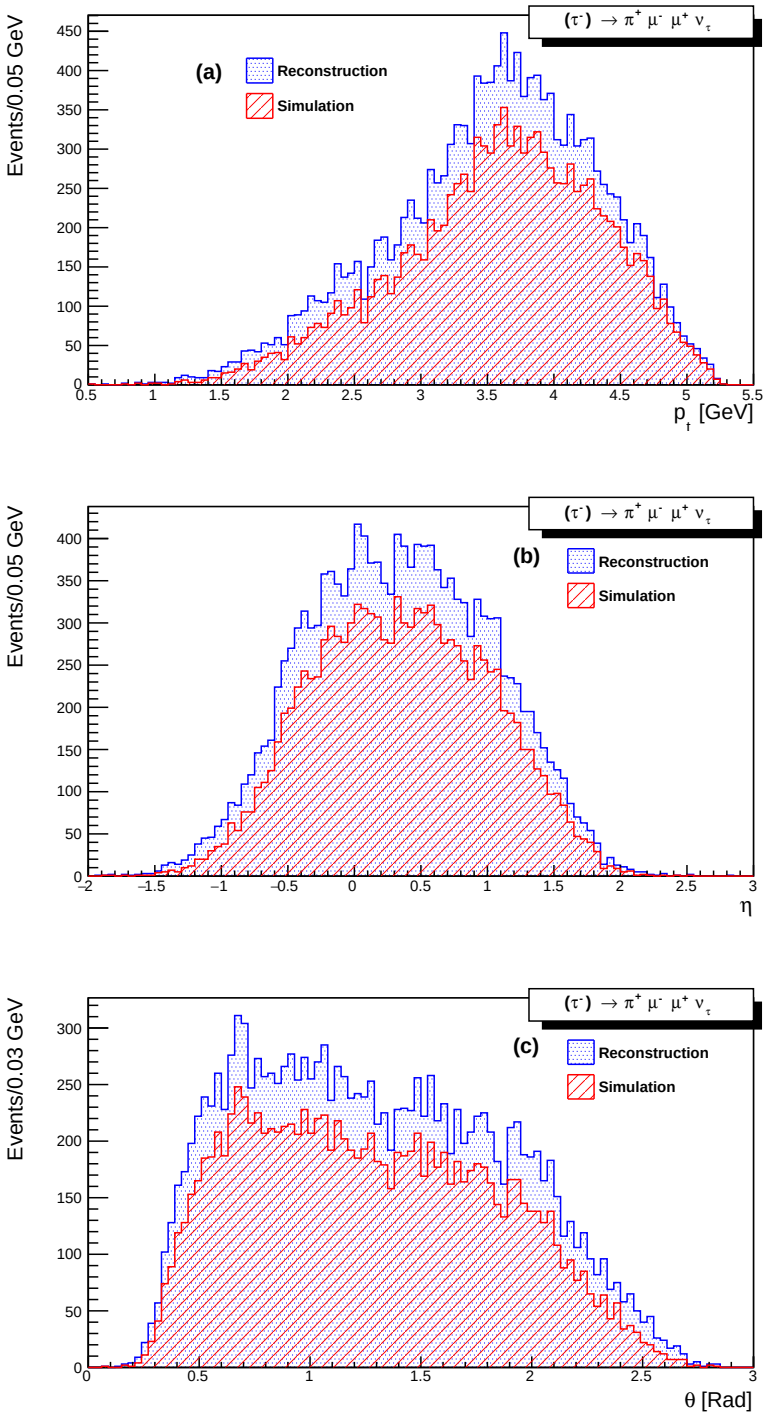

Figure 4.11: Transerve momentum (top), pseudorapidity (middle) and polar angle (bottom) for the decay channel $\tau^- \to \pi^+\mu^-\mu^+\nu_\tau$ with an invariant mass window of $1.0 < M_\tau < 1.9$ GeV, PID ($\mu > 20\%$ $\pi > 80\%$), $M_{bc} \leq 4$ GeV, using 13,208 reconstructed events (blue) and 10,834 simulated events (red).

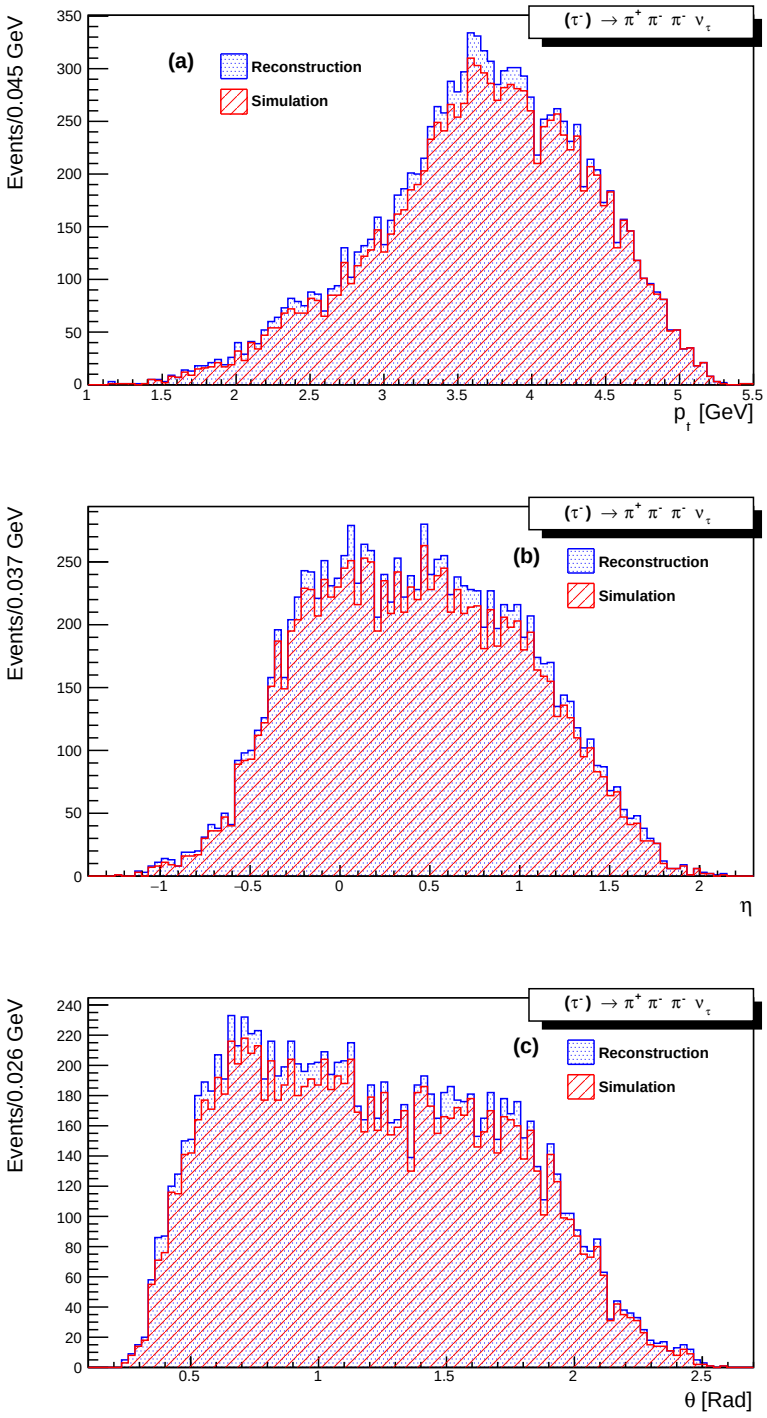

Figure 4.12: Transerve momentum (top), pseudorapidity (middle) and polar angle (bottom) for the decay channel $\tau^- \to \pi^+\pi^-\pi^-\nu_\tau$ with an invariant mass window of $1.0 < M_\tau < 1.9$ GeV, PID ($\pi > 80\%$), $M_{bc} \leq 4$ GeV, using 11,812 reconstructed events (blue) and 11,116 simulated events (red).

4.1.4 False signal

Finally, we consider the possibility to reconstruct wrongly events of interest. We used the background events and found the signal channel, we called them **false signals**. In the table 4.3 we can observe that $\tau^- \to \pi^+\mu^-\mu^+\nu_\tau$ channel is less efficient than $\tau^- \to \pi^+\pi^-\pi^-\nu_\tau$ channel so we should expect more false events.

We called false signal for each background

- Background 1: $\tau^- \to \pi^+\mu^-\mu^+\nu_\tau$
- Background 2: $\tau^- \to \pi^+\pi^-\pi^-\nu_\tau$

The used cuts in these searches were the same that we used to find the simulated signal: $1.0 < M < 1.9$ invariant mass window to reconstruct τ's; PID at $\geq 80\%$ and $\geq \%20$ for π's and μ's, respectively; and $M_{bc} \leq 4.0$ GeV. In **Table 4.4** we can see the amount of reconstructed events which correspond to false signals. In the $\tau^- \to \pi^+\mu^-\mu^+\nu_\tau$ channel there are more reconstructed events than in the $\tau^- \to \pi^+\pi^-\pi^-\nu_\tau$ channel.

False signal	$1.0 < M < 1.9$ and $M_{bc} \leq 4$GeV
$\tau^- \to \pi^+\mu^-\mu^+\nu_\tau$	2,825
$\tau^- \to \pi^+\pi^-\pi^-\nu_\tau$	537

Table 4.4: Reconstructed events; mass, PID and M_{bc} cuts are used.

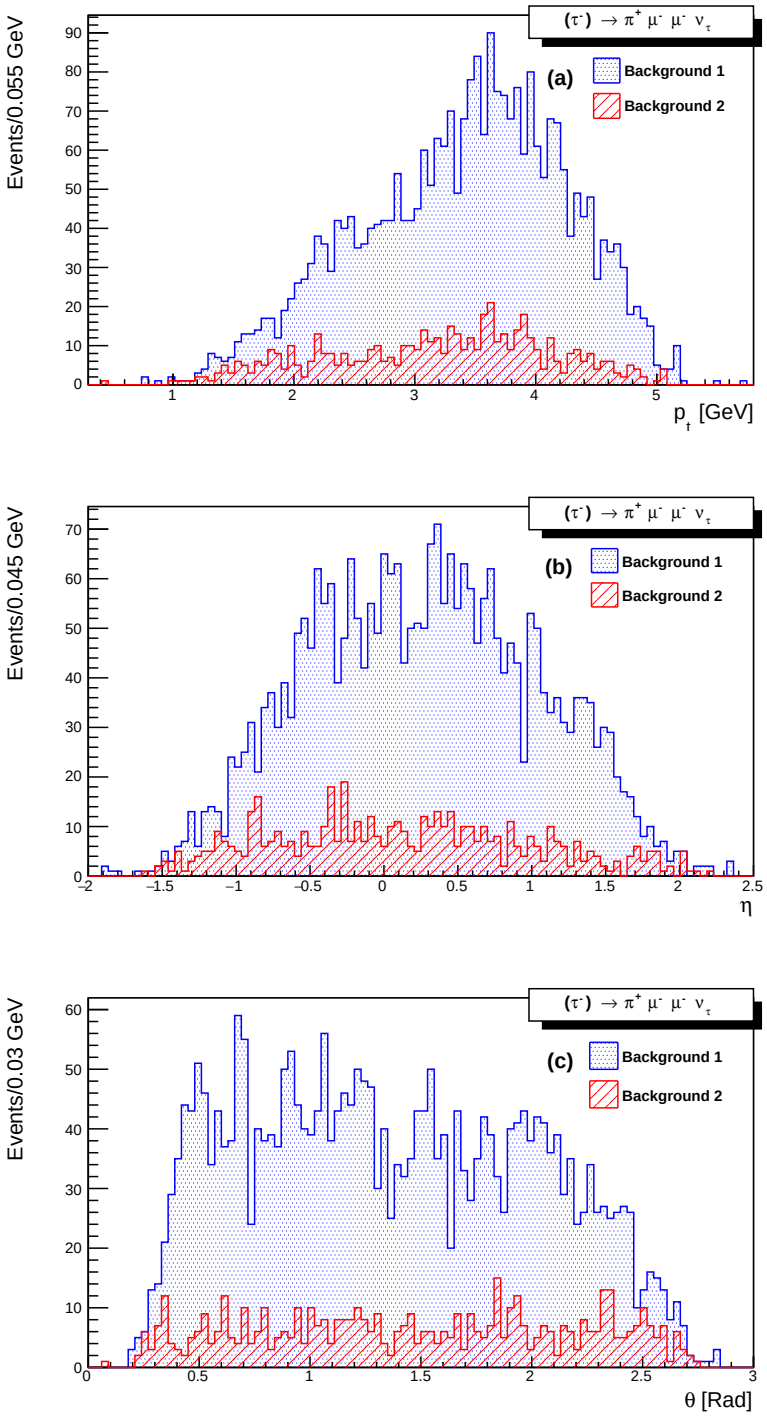

Figure 4.13: Transerve momentum (top), pseudorapidity (middle) and polar angle (bottom) for the decay channel $(\tau^-) \to \pi^+\mu^-\mu^-\nu_\tau$ with an invariant mass window of $1.0 < M_\tau < 1.9$ GeV, PID ($\mu > 20\%$ $\pi > 80\%$), $M_{bc} \leq 4$ GeV, using 2,825 for background 1 (blue) and 537 for background 2 (red).

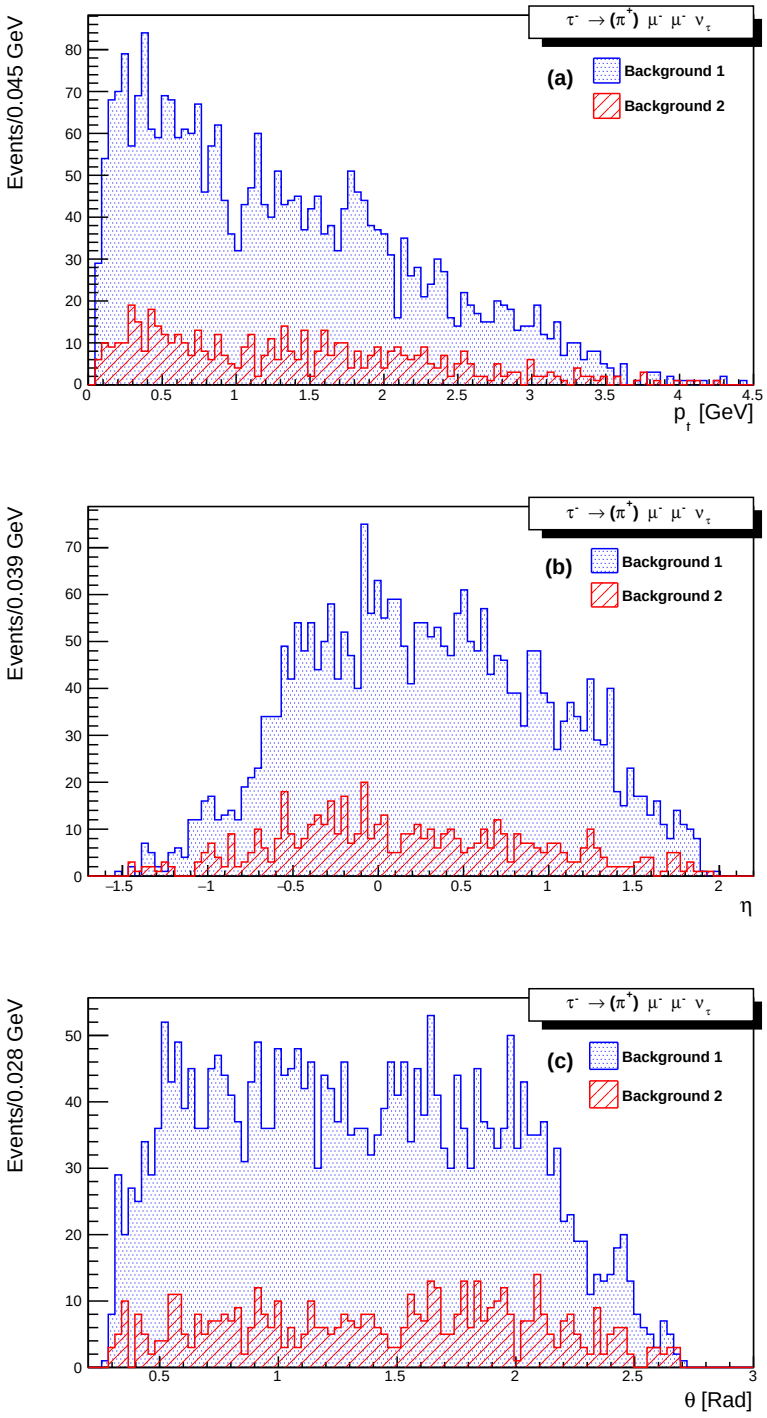

Figure 4.14: Transerve momentum (top), pseudorapidity (middle) and polar angle (bottom) for the decay channel $(\tau^-) \to (\pi^+)\mu^-\mu^-\nu_\tau$ with an invariant mass window of $1.0 < M_\tau < 1.9$ GeV, PID ($\mu > 20\%$ $\pi > 80\%$), $M_{bc} \leq 4$ GeV, using 2,825 for background 1 (blue) and 537 for background 2 (red).

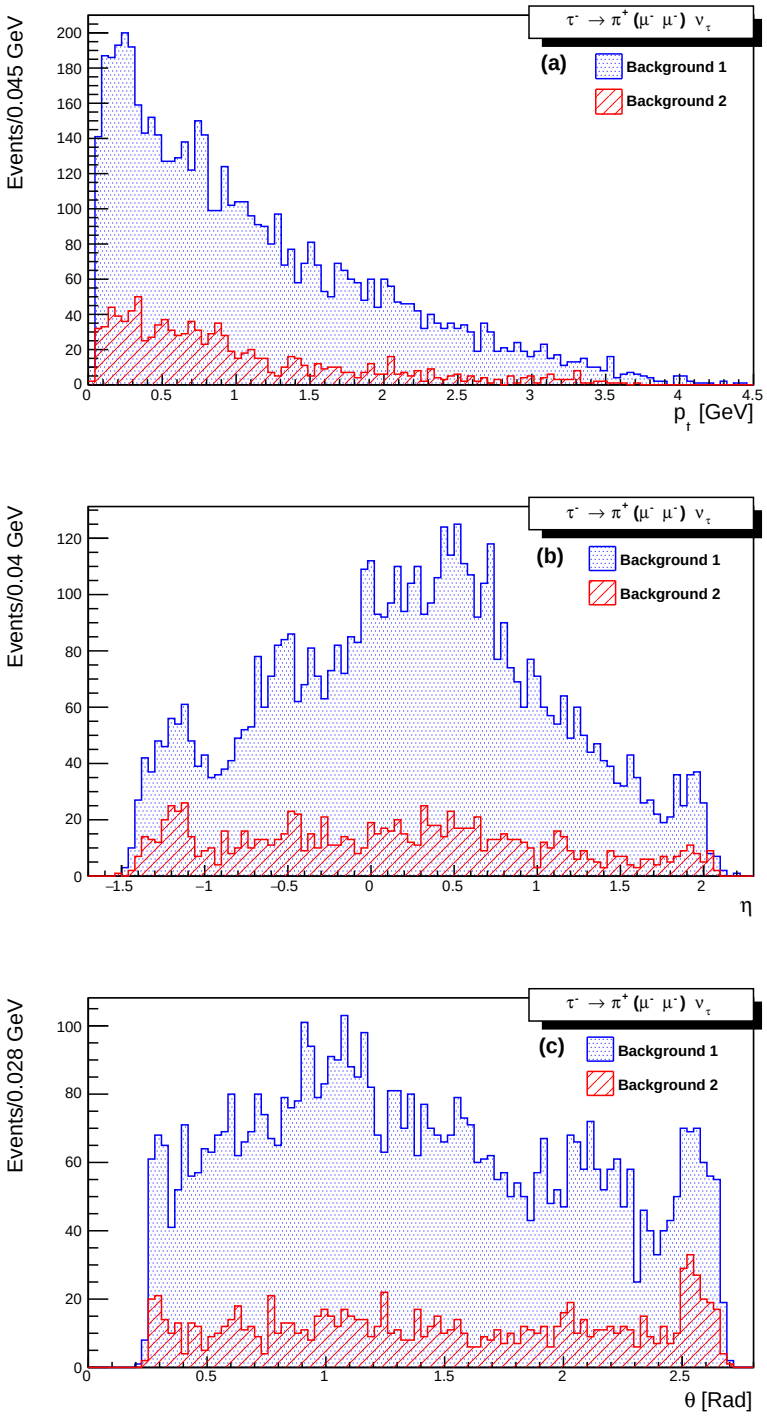

Figure 4.15: Transerve momentum (top), pseudorapidity (middle) and polar angle (bottom) for the decay channel $(\tau^-) \to \pi^+(\mu^-\mu^-)\nu_\tau$ with an invariant mass window of $1.0 < M_\tau < 1.9$ GeV, PID ($\mu > 20\%$ $\pi > 80\%$), $M_{bc} \leq 4$ GeV, using 5,650 for background 1 (blue) and 1,074 for background 2 (red).

We generated 50000 events for the channel of interest and used the invariant mass window, the particle identification in π's and μ's, and beam constrained mass to reconstruct the channel as well as possible.

The window should be as large as possible to reconstruct the 50,000 of simulated events. The PID of π's is less significant than μ's, and the beam constrained mass was the most important variable to reconstruct as well as possible the generated events. The figures 4.10, 4.11, and 4.12 show the channels studied.

- $\tau^- \to \pi^+\mu^-\mu^-\nu_\tau$
- $\tau^- \to \pi^+\mu^-\mu^+\nu_\tau$
- $\tau^- \to \pi^+\pi^-\pi^-\nu_\tau$

We consider the last two we consider as background, 50000 generated events in each case.

Finally, the total events reconstructed correctly were 11680, 10834, and 11116 for $\tau^- \to \pi^+\mu^-\mu^-\nu_\tau$, $\tau^- \to \pi^+\mu^-\mu^+\nu_\tau$, $\tau^- \to \pi^+\pi^-\pi^-\nu_\tau$, respectively. This is in agreement with the false signal (Figure 4.13) measured, 2825 and 537 events reconstructed wrongly for $\tau^- \to \pi^+\mu^-\mu^+\nu_\tau$ and $\tau^- \to \pi^+\pi^-\pi^-\nu_\tau$, respectively.

Chapter 5

Conclusions and plans

5.1 Conclusions

The Belle II will be an important experiment trying to answer the question about the neutrino nature. If neutrinos are Majorana particles we can use it to find violation of leptonic number processes.

However, Belle II is not working yet so we started with an analysis with simulated data. We simulated the channel (signal)

$$\tau^- \to \pi^+\mu^-\mu^-\nu_\tau$$

which is a decay to four bodies and its branching fraction is enhanced with respect to decays to three bodies, this was a great motivation. We studied the possibility to find the $\tau^- \to \pi^+\mu^-\mu^-\nu_\tau$ channel that violate the leptonic number by two units.

In order to have an approximation to real experiments or real data we used two set of variables: **Reconstruction data** and **Simulation data** (Section 4.1). Then, we considered the most general distribution in high energy physics (P_t, η and θ) to reconstruct them as well as possible (Figures 4.10, 4.11 and 4.12). Here, we observed the importance of some variables: the invariant mass cut that allowed us to have the necessary amount of reconstructed events; PID cuts (these cuts represent the efficiency of the detector to reconstruct π's and μ's), it was more sensitive to reconstruct μ's than π's; and M_{bc} cut, in this case one of the most important variables

due to the energy loss of neutrinos.

We generated 50000 events for the signal channel and the total events reconstructed correctly were 11680. Furthermore, we generated channels (50000 events for each channel) which were similar to the signal channel but they did not violate the leptonic number. The channels were $\tau^- \to \pi^+\mu^-\mu^+\nu_\tau$ and $\tau^- \to \pi^+\pi^-\pi^-\nu_\tau$ and we reconstructed correctly 10834 and 11116 events, respectively.

The study of similar channels (background) allowed us to know the possibility to wrongly reconstruct the signal channel (Figures 4.13, 4.14 and 4.15). We found wrongly 2825 and 537 signal events when the data corresponded to $\tau^- \to \pi^+\mu^-\mu^+\nu_\tau$ and $\tau^- \to \pi^+\pi^-\pi^-\nu_\tau$, respectively.

Despite the fact that we only reconstructed correctly 11680 of 50000 events for the signal channel, we can say that "it will be possible to find the $\tau^- \to \pi^+\mu^-\mu^-\nu_\tau$ channel that violate the leptonic number by two units in the Belle II experiment" indicating the Majorana nature discovery of the neutrinos. However, these words are only valid if all conditions considered to be held in this work are correct. But we know this is a naive affirmation due to that the fact we do not consider, for instance, all other decay channels of τ lepton and their branching fractions (larger in several cases) and the reconstruction efficiency.

5.2 Plans

We can improve the herein presented analysis using tools of *multivariate analysis*. Some available methods are: boosted decision trees, neural networks and likelihood functions. In general, they will allow us to combine several discriminating variables into one final as well as finding variable correlations that could exist.

On the other hand, we will have real data in three or four years to do this analysis so we can use the tools we have developed in further analyses.

Bibliography

[1] A.K. Mann, H. Primakoff, Phys. Rev. D **15**, 655 (1977). DOI 10.1103/PhysRevD.15.655. URL http://link.aps.org/doi/10.1103/PhysRevD.15.655

[2] W. Frati, T.K. Gaisser, A.K. Mann, T. Stanev, Phys. Rev. D **48**, 1140 (1993). DOI 10.1103/PhysRevD.48.1140. URL http://link.aps.org/doi/10.1103/PhysRevD.48.1140

[3] T.K. Kuo, J. Pantaleone, Phys. Rev. D **41**, 3842 (1990). DOI 10.1103/PhysRevD.41.3842. URL http://link.aps.org/doi/10.1103/PhysRevD.41.3842

[4] J. Ehlers, K. Hepp, E. Board, R. Beig, W. Domcke, U. Frisch, W. Hillebrandt, R.L. Jaffe, *Introduction to the Physics of Massive and Mixed Neutrinos*

[5] M. Goldhaber, L. Grodzins, A.W. Sunyar, Phys. Rev. **109**, 1015 (1958). DOI 10.1103/PhysRev.109.1015. URL http://link.aps.org/doi/10.1103/PhysRev.109.1015

[6] N. Quintero, Estudios de violación del número leptónico en procesos resonantes inducidos por un neutrino de mayorana. Ph.D. thesis (2014)

[7] F.T. Avignone, S.R. Elliott, J. Engel, Reviews of Modern Physics **80**(June), 481 (2008). DOI 10.1103/RevModPhys.80.481

[8] C.S. Wu, E. Ambler, R.W. Hayward, D.D. Hoppes, R.P. Hudson, Phys. Rev. **105**, 1413 (1957). DOI 10.1103/PhysRev.105.1413. URL http://link.aps.org/doi/10.1103/PhysRev.105.1413

[9] G. Danby, J.M. Gaillard, K. Goulianos, L.M. Lederman, N. Mistry, M. Schwartz, J. Steinberger, Phys. Rev. Lett. **9**, 36 (1962). DOI 10.1103/PhysRevLett.9.36. URL http://link.aps.org/doi/10.1103/PhysRevLett.9.36

[10] B.T. Cleveland, T. Daily, J. Raymond Davis, J.R. Distel, K. Lande, C.K. Lee, P.S. Wildenhain, J. Ullman, The Astrophysical Journal **496**(1), 505 (1998). URL http://stacks.iop.org/0004-637X/496/i=1/a=505

[11] F. et al, Phys. Rev. Lett. **77**, 1683 (1996). DOI 10.1103/PhysRevLett.77.1683. URL http://link.aps.org/doi/10.1103/PhysRevLett.77.1683

[12] C. et al, Phys. Rev. D **78**, 032002 (2008). DOI 10.1103/PhysRevD.78.032002. URL http://link.aps.org/doi/10.1103/PhysRevD.78.032002

[13] G. López Castro, N. Quintero, Phys. Rev. D **87**, 077901 (2013). DOI 10.1103/PhysRevD.87.077901. URL http://link.aps.org/doi/10.1103/PhysRevD.87.077901

[14] S.R. Elliott, P. Vogel, Annual Review of Nuclear and Particle Science **52**(1), 115 (2002). DOI 10.1146/annurev.nucl.52.050102.090641. URL http://dx.doi.org/10.1146/annurev.nucl.52.050102.090641

[15] J. Schechter, J.W.F. Valle, Phys. Rev. D **25**, 2951 (1982). DOI 10.1103/PhysRevD.25.2951. URL http://link.aps.org/doi/10.1103/PhysRevD.25.2951

[16] A. Ilakovac, Phys. Rev. D **54**, 5653 (1996). DOI 10.1103/PhysRevD.54.5653. URL http://link.aps.org/doi/10.1103/PhysRevD.54.5653

[17] S.M. Bilenky, pp. 690–715 (2010). DOI 10.1134/S1063779610050035. URL http://arxiv.org/abs/1001.1946

[18] J.J.G.C. et al, Phys. Rev. pp. 29–98 (2012). DOI 10.1393/ncr/i2012-10074-9

[19] O.S. Brüning, P. Collier, P. Lebrun, S. Myers, R. Ostojic, J. Poole, P. Proudlock, *LHC Design Report* (CERN, Geneva, 2004). URL https://cds.cern.ch/record/782076

[20] H. Hahn, E. Forsyth, H. Foelsche, M. Harrison, J. Kewisch, G. Parzen, S. Peggs, E. Raka, a. Ruggiero, a. Stevens, S. Tepikian, P. Thieberger, D. Trbojevic, J. Wei, E. Willen, S. Ozaki, S.Y. Lee, Nuclear Instruments and Methods in Physics Research, Section A: Accelerators, Spectrometers, Detectors and Associated Equipment **499**(2-3), 245 (2003). DOI 10.1016/S0168-9002(02)01938-1

[21] S. Choubey, et al., (2011)

[22] P.D.I.B. group), *Belle II, Technical Design Report* (2010)

[23] H. Sagawa, Il Nuovo Cimento A **109**(6-7), 1055 (1996). DOI 10.1007/BF02823646. URL http://dx.doi.org/10.1007/BF02823646

[24] K. Inami, Nucl. Instrum. Meth. **595** (2008). DOI http://dx.doi.org/10.1016/j.nima.2008.07.045. URL http://www.sciencedirect.com/science/article/pii/S0168900208009510

[25] A. Moll. The Software Framework of the Belle II Experiment (2011). DOI 10.1088/1742-6596/331/3/032024

[26] D.J. Lange, Nucl. Instrum. Meth. **A462**, 152 (2001). DOI 10.1016/S0168-9002(01)00089-4

[27] S. Jadach, (July 1999)

[28] Nuclear Instruments and Methods in Physics Research Section A: Accelerators, Spectrometers, Detectors and Associated Equipment **506**(3), 250 (2003). DOI http://dx.doi.org/10.1016/S0168-9002(03)01368-8. URL http://www.sciencedirect.com/science/article/pii/S0168900203013688

[29] R. Brun, F. Rademakers, Nuclear Instruments and Methods in Physics Research Section A: Accelerators, Spectrometers, Detectors and Assosiated Equipment pp. 81–86 (1997)

[30] S. Jadach, B.F.L. Ward, Z. Was, (March) (2000). DOI 10.1103/PhysRevD.63.113009. URL http://arxiv.org/abs/hep-ph/0006359

[31] S. Banerjee, B. Pietrzyk, J.M. Roney, Z. Was, Physical Review D - Particles, Fields, Gravitation and Cosmology **77**(5), 1 (2008). DOI 10.1103/PhysRevD.77.054012

[32] P.G. et al, URL http://wasm.home.cern.ch/wasm/",year="2000"

[33] T. Sjöstrand, S. Mrenna, P. Skands, Journal of High Energy Physics **2006**(05), 026 (2006). DOI 10.1088/1126-6708/2006/05/026. URL http://arxiv.org/abs/hep-ph/0603175$\delimiter"026E30F$nhttp://stacks.iop.org/1126-6708/2006/i=05/a=026?key=crossref.7fbc8fa1a47a48f7565bead655446685

[34] K.O. et al. (Particle Data Group), Chin. Phys. 090001 **C38** (2014). URL http://pdg.lbl.gov